

Effects of a semipervious lens on soil vapour extraction

By CHIU-ON NG AND CHIANG C. MEI

Department of Civil and Environmental Engineering, Massachusetts Institute of Technology,
Cambridge, MA 02139, USA

(Received 8 September 1996 and in revised form 20 February 1997)

We describe a theory for the removal of volatile organic chemicals from an unsaturated soil stratum consisting of highly porous coarse sand layers sandwiching a thin and semipervious lens. Each soil layer is modelled as a periodic array of spherical aggregates formed by solid grains and immobile water trapped by surface tension. Volatile chemicals are vaporized in the mobile air in pores between aggregates, dissolved in the intra-aggregate water, and adsorbed on the surface of soil grains. Using the effective transport equations derived for the aggregated soils, we consider shallow layers with sharp contrast in physical properties. An asymptotic analysis is developed for an axisymmetric geometry, yielding quasi-one-dimensional governing equations for individual layers. At the leading order the flow and the vapour transport are horizontal in the coarse layers but vertical in the semipervious lens. Numerical results are presented for a simple example to demonstrate the significance of the lens permeability, diffusivity and retardation factor, and the aggregate diffusivity in the coarse layers, on the vapour transport during the stages of contamination and air-venting.

1. Introduction

Non-aqueous-phase liquids leaked in an unsaturated or vadose zone often become a persistent source of contaminant vapour and groundwater contamination. The vapour of volatile organic compounds (VOC) can spread to large areas owing to the high mobility of the gaseous phase in pore space (Schwille 1988). Cleaning up the contaminated soil is difficult because the vapour is capable of partitioning into the soil moisture and the solid organic matter.

Removal of VOC vapour in the unsaturated zone is usually achieved by pumping the vapour-laden air in the pores into suction wells placed in the contaminated vadose zone. The process is usually called *soil vapour extraction* (SVE). As the vapour is removed, the aqueous and the sorbed phases will also be depleted, driven by phase change kinetics. Very often, unsaturated zones are stratified: layers of semipervious soil, such as clay lenses, are embedded in a medium of more porous or sandy materials. Obviously if SVE is applied in such a heterogeneous system, the progress of the remediation is likely to be limited by the slow removal rate of contaminant in the low-permeability layers. To provide guidance for designing SVE in a layered soil, it is necessary to develop an effective vapour transport model which takes into account the difference in flow and transport capacity of individual layers.

Most existing models for the vapour transport in an unsaturated zone are focused on homogeneous soils. In earlier works (e.g. Abriola & Pinder 1985; Corapcioglu

& Baehr 1987; Kaluarachchi & Parker 1990), the emphasis is to develop multiphase transport models for groundwater contamination which consider only diffusive vapour transport. The effects of density-driven advection of dense vapour were later studied by Sleep & Sykes (1989), Falta *et al.* (1989) and Mendoza & Frind (1990). SVE is distinguished by the fact that vapour advection is forced by pumping. Typical works in this category include Wilson, Clarke & Clarke (1988), Baehr, Hoag & Marley (1989), Johnson, Kemblowski & Colthart (1990a), Rathfelder, Yeh & Mackay (1991) and Falta, Pruess & Chesnut (1993). These models ignore the kinetics of inter-phase mass transfer and assume that all phase partitionings are always in local equilibrium. Evidence of transfer kinetics has nevertheless been found in some experimental observations. This motivated the kinetic models by Sleep & Sykes (1989), Brusseau (1991) and Armstrong, Frind & McClellan (1994) who adopt first-order relations to describe the inter-phase mass transfer rates on the macro-scale. The first-order rate constants are essentially empirical: in most cases definite data are not available and are difficult to estimate. A more theoretically satisfactory alternative is the spherical aggregate diffusion model (e.g. Brusseau & Rao 1990; Gierke, Hutzler & McKenzie 1992) for which the governing equations can be justified rigorously (Ng & Mei 1996a). With constitutive coefficients known from reliable experimental data, this model has been confirmed by one-dimensional experiments in a packed soil column (Ng & Mei 1996b).

Studies on the effects of soil heterogeneity on SVE have been rather limited. Johnson *et al.* (1990a,b) presented one-dimensional mass-transfer-limited models for steady vapour transport on top of a layer of liquid VOC or a layer of low-permeability soil with residual liquid hydrocarbon. Experimental and theoretical investigations of a similar problem were carried out by Ho & Udell (1991, 1992), who provide visual evidence of the geometrical evolution of a liquid VOC pool in a low-permeability layer as a result of overhead air blowing. Contrasting features of air flow and vapour transport in different layers are however not studied in these works.

The objective of the present study is to examine theoretically the effects of soil stratification on the flow of pore air and the transport of volatile chemicals in an SVE operation. Letting each layer be formed by spherical aggregates, we shall derive approximate equations that capture the essential physics for a shallow coarse soil stratum with a thin fine-grained lens of very low permeability. The coarse- and fine-grained layers are assumed to have sharply contrasting air conductivities and vapour diffusivities. While the contaminant source is confined to a small region in the coarse layer above the lens, the vapour is allowed to spread laterally before pumping to great distances. We assume that density-driven advection is not important. This is true for compounds like toluene and xylene which have a relatively small molecular weight and a low vapour pressure at soil temperatures (Falta *et al.* 1989).

In §2, we shall give the basic equations and boundary conditions. Scales of various physical parameters are estimated in §3. Based on the small ratio of characteristic length scales which is also related to the permeability ratio, a perturbation analysis is carried out in §4 and yields the leading-order governing equations and boundary conditions. The asymptotic procedure resembles that used previously in deriving the seepage equation for finite strain consolidation in an aquifer-aquitard-aquifer system (Fallou, Mei & Lee 1992; Lee, Fallou & Mei 1992; Ng & Mei 1995). It will be seen that the sharp contrast of material properties helps to simplify the spatial dependence in both flow and transport problems. Numerical solutions of the asymptotic equations are discussed in §5. Attention will be focused on the effects of the soil properties (conductivity, diffusivity and retardation factor), aggregate diffusion

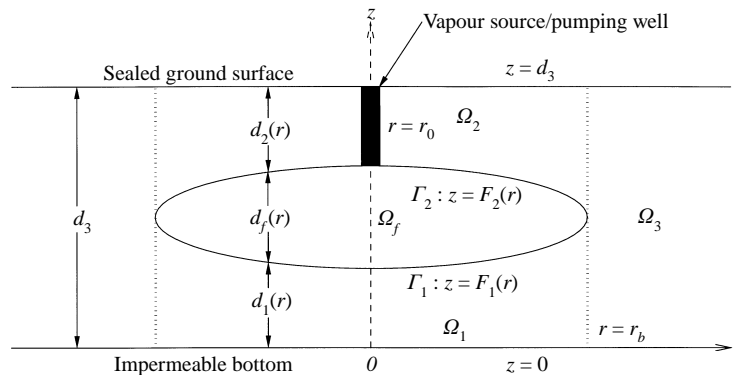


FIGURE 1. Definition sketch of problem geometry.

rate and pumping strength on the vapour distribution as a function of space and time.

2. Problem formulation

As shown in figure 1, the unsaturated zone consists of a confined and horizontal stratum of coarse and highly permeable soil sandwiching a thin lens of much finer and semipervious soil. To study the physics without excessive computation, axial symmetry about the centre of the lens is assumed. With its top and bottom surfaces being well-sealed, the unsaturated zone is assumed to extend radially to infinity. Practically a sealed ground surface is desirable for SVE in order to control the air flow to pass through the contaminated soils (e.g. Johnson *et al.* 1990b). The case with an underlying saturated zone is not treated in this study. The moisture content in the unsaturated zone is assumed to be at the irreducible level so that in the absence of surface recharge the pore water is not draining. A cylindrical coordinate system (r, z) is defined as shown in figure 1.

We denote the semipervious lens by Ω_f (where the subscript f stands for fine grains), its lower surface by $\Gamma_1: z = F_1(r)$, its upper surface by $\Gamma_2: z = F_2(r)$, and its maximum radius by $r = r_b$. For convenience of identification the coarse zone is divided into three layers: the inner layers below (Ω_1) and above (Ω_2) the lens, and the outer layer Ω_3 . The thicknesses d_1 , d_2 and d_f of Ω_1 , Ω_2 and Ω_f respectively are functions of r , while the total thickness d_3 of the soil stratum is assumed to be constant. We also assume that within each layer the soil is isotropic, though not necessarily homogeneous.

We suppose that initially ($t < 0$) the soil is clean. At the instant $t = 0$ a VOC-contaminated soil column is introduced at the centre and fully penetrates the upper layer Ω_2 . The vapour concentration in the soil column is maintained at a constant level for the duration $0 < t < T$, while vapour diffuses continuously into the surrounding soil. At $t = T > 0$, the contaminated soil column is replaced by a vacuum well, in which the pressure is lowered in order to withdraw air from the surrounding soil. Variations of VOC vapour concentration as a function of time and space are to be sought.

On the pore scale, each soil layer is assumed to be packed by uniform spherical aggregates inside which water is held immobilized by capillary forces. Air containing the vapour phase of a chemical fills and moves in the pore space between the

aggregates. The same chemical is also dissolved in the intra-aggregate water, and adsorbed on the particles constituting the aggregates. We further assume equilibrium chemical partitioning between aqueous and sorbed phases inside an aggregate, and also between vapour and aqueous phases on the air/aggregate interface. Note that these are local assumptions on the aggregate scale and differ from the usual assumption of local equilibrium on the macro-scale.

2.1. Governing equations

For demonstrating our basic ideas, it suffices to consider the case of axial symmetry. We begin with the exact equations for the air flow and the vapour transport applicable to all layers. Because the externally applied pressure change can be significant, air can be compressible and must satisfy the continuity equation:

$$\theta_g \frac{\partial \rho}{\partial t} + \frac{1}{r} \frac{\partial}{\partial r} (r \rho u) + \frac{\partial}{\partial z} (\rho w) = 0 \quad (2.1)$$

where t is the time, (u, w) are the radial and the vertical components of the specific discharge (i.e. flow per unit area of soil matrix), ρ is the air density, and θ_g is the macro-porosity (i.e. the volume fraction of air-filled pore space) of the medium. The specific discharge is related to the pressure gradient according to Darcy's law:

$$(u, w) = -k \left(\frac{\partial p}{\partial r}, \frac{\partial p}{\partial z} \right) \quad (2.2)$$

where p is the absolute air pressure, and k is the air conductivity of the medium divided by the air specific weight. The gravity effect is ignored in (2.2). This is justifiable during pumping since the applied pressure gradient will dominate. Before pumping, the buoyancy effect is also negligible compared to diffusion when the chemical has a relatively small molecular weight and its vapour pressure is much lower than the atmospheric pressure (Falta *et al.* 1989).

Modelling air as an ideal gas, the equation of state reads

$$\frac{pM}{R_g \Theta} = \rho \quad (2.3)$$

where M is the molecular weight of the air mixture, R_g is the universal gas constant, and Θ is the absolute air temperature. We assume that both Θ and M are constants so that p is linearly proportional to ρ . Note that we shall not distinguish the air pressure from the total gas pressure, since the partial pressure due to VOC vapour is assumed to be relatively small. Limiting to these conditions, a nonlinear equation for p follows by inserting (2.2) into (2.1):

$$\theta_g \frac{\partial p}{\partial t} - \frac{1}{r} \frac{\partial}{\partial r} \left(r k p \frac{\partial p}{\partial r} \right) - \frac{\partial}{\partial z} \left(k p \frac{\partial p}{\partial z} \right) = 0. \quad (2.4)$$

Note that the above flow equation is independent of chemical vapour transport and can be solved in advance.

We adopt the so-called aggregate-diffusion model where the soil in each layer is composed of a regular array of spherical aggregates of equal radius a . The aqueous diffusivity inside an aggregate (D_w) is assumed to be very small compared to the vapour diffusivity in the pore air (D) (e.g. see Brusseau & Rao 1990; Ng & Mei

1996a,b; and references cited therein). The equation for the vapour transport is

$$\theta_g \frac{\partial c_g}{\partial t} + \frac{1}{r} \frac{\partial}{\partial r}(r u c_g) + \frac{\partial}{\partial z}(w c_g) - \frac{1}{r} \frac{\partial}{\partial r} \left(r D \frac{\partial c_g}{\partial r} \right) - \frac{\partial}{\partial z} \left(D \frac{\partial c_g}{\partial z} \right) = - \frac{6\phi D_w \theta_a}{a^2 H} \sum_{n=1}^{\infty} \int_0^t e^{-\lambda_n(t-\tau)} \frac{\partial c_g}{\partial \tau} d\tau, \quad (2.5)$$

where the time integral on the right-hand side represents the mass transfer rate from aggregates into pore air per bulk soil volume. In this equation, the vapour concentration $c_g(r, z, t)$ is defined as the mass of chemical vapour per phase volume, ϕ is the intra-aggregate porosity, $\theta_a = 1 - \theta_g$ is the volume fraction of aggregates, and H is Henry's law constant. Also,

$$\lambda_n = n^2 \pi^2 D_e / a^2 \quad (n = 1, 2, \dots), \quad (2.6)$$

where

$$D_e = \frac{\phi D_w}{K_d(1 - \phi)\rho_s + \phi} \quad (2.7)$$

is the sorption-retarded effective diffusivity in an aggregate, in which K_d is the sorption partition coefficient, and ρ_s is the aggregate solid density. The aqueous concentration in aggregates, c_w , is in general not in equilibrium with the vapour concentration, and its mean value over an aggregate volume can be found from

$$\bar{c}_w = \frac{1}{H} \left[c_g - \frac{6D_e}{a^2} \sum_{n=1}^{\infty} \int_0^t \frac{e^{-\lambda_n(t-\tau)}}{\lambda_n} \frac{\partial c_g}{\partial \tau} d\tau \right]. \quad (2.8)$$

Equations (2.5) and (2.8) hold for each layer, coarse or fine, and have been derived rigorously by the theory of homogenization (Ng & Mei 1996a).

2.2. Boundary conditions

Referring to figure 1, let us distinguish by the subscripts $i = 1, 2$ quantities for the two coarse layers below and above the lens respectively, and by $i = 3$ the coarse layer outside the vertical cylinder containing the lens. The subscript f is used to distinguish the fine-grained semipervious lens. First, at the centre of the bottom coarse layer Ω_1 , the pressure and the concentration gradients are zero by axial symmetry:

$$\frac{\partial p_1}{\partial r} = 0, \quad \frac{\partial c_{g1}}{\partial r} = 0 \quad \text{at } r = 0, \quad 0 < z < F_1(r), \quad 0 < t. \quad (2.9)$$

At the outer radius of the centre column of radius r_0 , i.e. the well screen, in the upper coarse layer Ω_2 , the boundary condition depends on the stage of operation. During the state of contamination, $0 < t < T$, there is no flow but a constant vapour concentration c_{g0} at $r = r_0$:

$$\frac{\partial p_2}{\partial r} = 0, \quad c_{g2} = c_{g0} \quad \text{at } r = r_0, \quad F_2(r) < z < d_3, \quad 0 < t < T. \quad (2.10)$$

During pumping, $t > T$, the pressure is equal to that in the well, p_0 , which is below the atmospheric pressure P_a . The concentration in the well is uniform so that there is

no concentration gradient. Thus

$$p_2 = p_0, \quad \frac{\partial c_{g2}}{\partial r} = 0 \quad \text{at } r = r_0, \quad F_2(r) < z < d_3, \quad T < t. \quad (2.11)$$

On the cylindrical interface between the outer coarse zone Ω_3 and the two inner coarse zones Ω_1 and Ω_2 , we require the continuity of pressure, concentration, and fluxes of air and vapour:

$$p_3 = p_1, \quad c_{g3} = c_{g1}, \quad \frac{\partial p_3}{\partial r} = \frac{\partial p_1}{\partial r}, \quad \frac{\partial c_{g3}}{\partial r} = \frac{\partial c_{g1}}{\partial r} \quad \text{at } r = r_b, \quad 0 < z < F_1(r), \quad (2.12)$$

$$p_3 = p_2, \quad c_{g3} = c_{g2}, \quad \frac{\partial p_3}{\partial r} = \frac{\partial p_2}{\partial r}, \quad \frac{\partial c_{g3}}{\partial r} = \frac{\partial c_{g2}}{\partial r} \quad \text{at } r = r_b, \quad F_2(r) < z < d_3. \quad (2.13)$$

Let the bottom of Ω_1 and Ω_3 and the top of Ω_2 and Ω_3 be impermeable; the normal fluxes are then zero there:

$$\frac{\partial p}{\partial z} = 0, \quad \frac{\partial c_g}{\partial z} = 0 \quad \text{at } z = 0 \text{ and } z = d_3, \quad 0 < r < \infty. \quad (2.14)$$

Along the lens boundaries Γ_1 , i.e. $z = F_1(r)$, $r < r_b$ and Γ_2 , i.e. $z = F_2(r)$, $r < r_b$, we also require the continuity of pressure, concentration, and normal fluxes of air and vapour:

$$p_i = p_f, \quad c_{gi} = c_{gf} \quad \text{on } \Gamma_i (i = 1, 2), \quad (2.15)$$

$$k_i \frac{\partial p_i}{\partial r} n_r + k_i \frac{\partial p_i}{\partial z} n_z = k_f \frac{\partial p_f}{\partial r} n_r + k_f \frac{\partial p_f}{\partial z} n_z \quad \text{on } \Gamma_i (i = 1, 2), \quad (2.16)$$

$$\begin{aligned} & \left(u_i c_{gi} - D_i \frac{\partial c_{gi}}{\partial r} \right) n_r + \left(w_i c_{gi} - D_i \frac{\partial c_{gi}}{\partial z} \right) n_z \\ & = \left(u_f c_{gf} - D_f \frac{\partial c_{gf}}{\partial r} \right) n_r + \left(w_f c_{gf} - D_f \frac{\partial c_{gf}}{\partial z} \right) n_z \quad \text{on } \Gamma_i (i = 1, 2), \end{aligned} \quad (2.17)$$

where (n_r, n_z) are the radial and the vertical components of the normal vector to the lens surface $\Gamma_i : z = F_i$ given by

$$(n_r, n_z) = (-\partial F_i / \partial r, 1). \quad (2.18)$$

Finally, at a large radial distance from the centre, the pressure is equal to the atmospheric pressure P_a and the vapour concentration is zero:

$$p_3 = P_a, \quad c_{g3} = 0 \quad \text{at } r \rightarrow \infty, \quad 0 < z < d_3. \quad (2.19)$$

For heterogeneous soils the three-dimensional equations and boundary conditions of this section are however unwieldy for computations and unrevealing for physical understanding. We shall therefore seek approximations for situations emulating some aspects of reality.

3. Estimates of scales

To provide a basis for perturbation analysis we first estimate the scales of important physical variables, and the relationship between some dimensionless ratios. All scales will be distinguished by tildes, i.e. the scale of f is \tilde{f} . For convenience, we summarize in table 1 the scales discussed below which will be used for normalization in later sections.

3.1. Geometrical shallowness

The radial length scale \tilde{r} , characterized by the maximum radius of the semipervious lens, is assumed to be much larger than the vertical length scale \tilde{d} , typical of a layer depth. We define the square of their ratio as the small ordering parameter:

$$\delta \equiv (\tilde{d}/\tilde{r})^2 \ll 1. \quad (3.1)$$

3.2. Radius of influence and conductivity contrast

Let \tilde{r}_p be the radius of influence, which is the radial length scale over which the pressure change in response to air pumping is significant. By balancing the radial flux through the pumping coarse layer and the vertical flux through the semipervious layer, it can be shown that the radius of influence is related to the permeability ratio (Lee *et al.* 1992):

$$\tilde{d}/\tilde{r}_p = (\tilde{k}_f/\tilde{k}_c)^{1/2} \quad (3.2)$$

where \tilde{k}_f and \tilde{k}_c are respectively the scales of the air conductivity of the semipervious lens and the coarse zone. The conductivity of air in soil is known to vary over a wide range of values. Typically for coarse materials $\tilde{k}_c = O(10^{-7}-10^{-9}) \text{ m}^2 (\text{Pa s})^{-1}$ and for fine materials $\tilde{k}_f = O(10^{-11}-10^{-13}) \text{ m}^2 (\text{Pa s})^{-1}$. Thus the ratio \tilde{k}_f/\tilde{k}_c varies over a broad range of small values $10^{-6}-10^{-2}$. However, we shall for generality assume that the conductivity ratio is such that the radius of influence is comparable to the radial geometrical length scale:

$$\tilde{r}_p = O(\tilde{r}). \quad (3.3)$$

It then follows from (3.1) and (3.2) that

$$\delta_k \equiv \tilde{k}_f/\tilde{k}_c = O(\delta). \quad (3.4)$$

3.3. Contrast of effective diffusivities in pore air

The effective diffusivity in pore air (D) varies with the air saturation and the total porosity of the medium according to the Millington formula (Millington 1959):

$$D/D_{\text{pure}} = (\text{air saturation})^{10/3} (\text{total porosity})^{4/3} \quad (3.5)$$

where D_{pure} is the diffusivity in pure air. Typically both air saturation and total porosity are larger in the coarse medium than the fine medium, and therefore D may differ appreciably in different media. For example, consider an air saturation of 0.8 and a total porosity of 0.5 for a coarse medium, and an air saturation of 0.2 and a total porosity of 0.2 for a fine medium. Then the above ratio is 0.19 for the coarse medium, but has a much smaller value of 5.5×10^{-4} for the fine medium. In this study we assume that the material contrast is sufficiently large such that

$$\delta_D \equiv \tilde{D}_f/\tilde{D}_c = O(\delta), \quad (3.6)$$

where \tilde{D}_f and \tilde{D}_c are respectively the scales of the effective vapour diffusivity in the semipervious lens and in the coarse layers.

3.4. Air specific discharge

Owing to the large conductivity contrast, the air specific discharge will have different scales in the two zones, and in different directions. Let $(\tilde{u}_c, \tilde{w}_c)$ and $(\tilde{u}_f, \tilde{w}_f)$ be respectively the scales of the specific discharge in the coarse layers and in the semipervious lens. From Darcy's law, we may estimate that the two radial components

are given by

$$\tilde{u}_c = -O(\tilde{k}_c \Delta \tilde{p} / \tilde{r}_p), \quad (3.7)$$

$$\tilde{u}_f = -O(\tilde{k}_f \Delta \tilde{p} / \tilde{r}_p) = O(\delta \tilde{u}_c), \quad (3.8)$$

where $\Delta \tilde{p} = P_a - p_0$ is the scale of the pressure drop in the well. While the radial specific discharges of air in the two zones differ by an order of δ , the vertical ones are comparable to each other by virtue of continuity. It is well-known that in a horizontally layered system with a sharp contrast in k the effective vertical conductivity of the composite is dominated by the conductivity of the less pervious layer. Therefore

$$\tilde{w}_c = \tilde{w}_f = -O(\tilde{k}_f \Delta \tilde{p} / \tilde{d}) = O(\delta^{1/2} \tilde{u}_c) \quad (3.9)$$

where the last equality is obtained by (3.1), (3.3) and (3.4). On combination of (3.8) and (3.9) it is clear that the flow is predominantly horizontal in a coarse layer, but almost vertical in the lens. For normalization purposes, the radial velocity scale is taken to be a positive number defined by

$$\tilde{u}_c = \tilde{k}_c (P_a - p_0) / \tilde{r}, \quad (3.10)$$

which varies with the well pressure p_0 . We also use the pressure drop in the well $P_a - p_0$ as the scale of pressure deviation from the atmospheric pressure.

A dimensionless parameter characterizing the flow rate is the Péclet number in the coarse layers, defined by

$$Pe \equiv \tilde{u}_c \tilde{r} / \tilde{D}_c = \tilde{k}_c (P_a - p_0) / \tilde{D}_c, \quad (3.11)$$

where the second equality is obtained using (3.10). Assuming $P_a - p_0$ is a finite fraction of $P_a = O(10^5 \text{ Pa})$, and using $\tilde{D}_c = O(0.1 \text{ cm}^2 \text{ s}^{-1})$ and $\tilde{k}_c = O(10^{-7} - 10^{-9} \text{ m}^2 (\text{Pa s})^{-1})$, we estimate that $Pe = O(10 - 10^3)$. Though the Péclet number can be large, it is desirable for generality to obtain a transport equation in which the diffusion is as important as the advection. Therefore we assume that

$$Pe \geq O(1). \quad (3.12)$$

3.5. Time scale

The advection time over a global distance along a coarse layer is given by $\tilde{t} = \tilde{r} / \tilde{u}_c$ which, by virtue of the above assumptions, is also comparable to

(i) the advection time scale across a coarse layer or the lens:

$$\tilde{t} = (\tilde{r} / \tilde{d})(\tilde{w}_c / \tilde{u}_c)(\tilde{d} / \tilde{w}_c) = O(\tilde{d} / \tilde{w}_c) = O(\tilde{d} / \tilde{w}_f); \quad (3.13)$$

(ii) the diffusion time scale across the lens:

$$\tilde{t} = (\tilde{r} / \tilde{d})^2 (\tilde{D}_c / \tilde{u}_c \tilde{r})(\tilde{D}_f / \tilde{D}_c)(\tilde{d}^2 / \tilde{D}_f) = O(\tilde{d}^2 / \tilde{D}_f); \quad (3.14)$$

and

(iii) the diffusion time over a global distance along a coarse layer:

$$\tilde{t} = (\tilde{D}_c / \tilde{u}_c \tilde{r})(\tilde{r}^2 / \tilde{D}_c) = O(\tilde{r}^2 / \tilde{D}_c). \quad (3.15)$$

In addition, we assume for generality that \tilde{t} is also comparable to the diffusion time across an aggregate in the coarse layers:

$$\tilde{t} = O(a_c^2 / D_{wc}) \quad (3.16)$$

Variable or parameter	Normalization scale
r, r_0, r_b	\tilde{r}
z, d_i, d_j, F_j	$\tilde{d} = \delta^{1/2}\tilde{r}$
k_i	\tilde{k}_c
k_f	$\tilde{k}_f = \delta_k \tilde{k}_c$
D_i	\tilde{D}_c
D_f	$\tilde{D}_f = \delta_D \tilde{D}_c$
u_i	$\tilde{u}_c = \tilde{k}_c(P_a - p_0)/\tilde{r}$
u_f	$\delta \tilde{u}_c$
w_i, w_f	$\delta^{1/2}\tilde{u}_c$
t, T	$\tilde{t} = \tilde{r}/(\tilde{u}_c \hat{P}_a)$
c_{gi}, c_{gf}	c_{g0}
c_w	c_{g0}/H
p'_i, p'_f	$P_a - p_0$

TABLE 1. Normalization scales ($i = 1, 2, 3, j = 1, 2$)

where a_c denotes the aggregate radius and D_{wc} is the aqueous diffusivity in an aggregate, both for the coarse layers. In summary only one distinct time scale \tilde{t} will be pertinent in the present problem.

To facilitate discussions on the evolution of the vapour plume prior to pumping, it is however desirable to use a time scale which is independent of the pumping pressure. Therefore we redefine the time scale as

$$\tilde{t} = \tilde{r}/(\tilde{u}_c \hat{P}_a) = \tilde{r}^2/(\tilde{k}_c P_a) \tag{3.17}$$

where P_a is the atmospheric pressure, and

$$\hat{P}_a = P_a/(P_a - p_0) = 1/(1 - p_0/P_a) \tag{3.18}$$

is the dimensionless parameter characterizing the well pressure, which is assumed to be of order unity. Note that the time scale for the flow to approach steady state is also given by (3.17), which as shown in (3.13)–(3.15) is comparable to the transport time scales. Therefore in the present transport problem the flow must be considered as transient. This is different from the case of open ground surface in which steady air flow can be established in a much shorter time scale than the transport processes (Ng & Mei 1996a).

4. Perturbation equations

We shall now deduce asymptotic expansions of the flow and the transport equations. The generic expansion of an unknown variable f is expanded in a power series of δ as follows:

$$f = f^{(0)} + \delta f^{(1)} + \delta^2 f^{(2)} + \dots \tag{4.1}$$

All normalized quantities will be distinguished by hats.

4.1. Air flow

Since the pressure drop in the well $P_a - p_0$ governs the pressure change in the soil layers, let us introduce the pressure deviation p' by

$$p'(r, z, t) \equiv P_a - p(r, z, t), \tag{4.2}$$

and define the normalized pressure deviation by

$$\hat{p}'(\hat{r}, \hat{z}, \hat{t}) = p'(r, z, t)/(P_a - p_0). \quad (4.3)$$

After changing the variable, we normalize the flow equation (2.4) and the interface condition (2.16) according to the scales in table 1:

$$\delta\theta_{gi}\hat{P}_a\frac{\partial\hat{p}'_i}{\partial\hat{t}} - \frac{\delta}{\hat{r}}\frac{\partial}{\partial\hat{r}}\left[\hat{r}\hat{k}_i(\hat{P}_a - \hat{p}'_i)\frac{\partial\hat{p}'_i}{\partial\hat{r}}\right] - \frac{\partial}{\partial\hat{z}}\left[\hat{k}_i(\hat{P}_a - \hat{p}'_i)\frac{\partial\hat{p}'_i}{\partial\hat{z}}\right] = 0 \quad \text{in } \Omega_i (i = 1, 2, 3), \quad (4.4)$$

$$\delta\theta_{gf}\hat{P}_a\frac{\partial\hat{p}'_f}{\partial\hat{t}} - \frac{\delta\delta_k}{\hat{r}}\frac{\partial}{\partial\hat{r}}\left[\hat{r}\hat{k}_f(\hat{P}_a - \hat{p}'_f)\frac{\partial\hat{p}'_f}{\partial\hat{r}}\right] - \delta_k\frac{\partial}{\partial\hat{z}}\left[\hat{k}_f(\hat{P}_a - \hat{p}'_f)\frac{\partial\hat{p}'_f}{\partial\hat{z}}\right] = 0 \quad \text{in } \Omega_f, \quad (4.5)$$

$$-\delta\hat{k}_i\frac{\partial\hat{p}'_i}{\partial\hat{r}}\frac{\partial\hat{F}_i}{\partial\hat{r}} + \hat{k}_i\frac{\partial\hat{p}'_i}{\partial\hat{z}} = -\delta\delta_k\hat{k}_f\frac{\partial\hat{p}'_f}{\partial\hat{r}}\frac{\partial\hat{F}_i}{\partial\hat{r}} + \delta_k\hat{k}_f\frac{\partial\hat{p}'_f}{\partial\hat{z}} \quad \text{on } \Gamma_i (i = 1, 2). \quad (4.6)$$

Recall that $\delta_k = O(\delta)$. We obtain perturbation equations by expanding the pressure deviations \hat{p}'_i and \hat{p}'_f according to (4.1).

In the coarse zone $\Omega_i (i = 1, 2, 3)$, the first two orders of the flow equation follow from (4.4):

$$-\frac{\partial}{\partial\hat{z}}\left[\hat{k}_i(\hat{P}_a - \hat{p}'_i^{(0)})\frac{\partial\hat{p}'_i^{(0)}}{\partial\hat{z}}\right] = 0, \quad (4.7)$$

and

$$\begin{aligned} \theta_{gi}\hat{P}_a\frac{\partial\hat{p}'_i^{(0)}}{\partial\hat{t}} - \frac{1}{\hat{r}}\frac{\partial}{\partial\hat{r}}\left[\hat{r}\hat{k}_i(\hat{P}_a - \hat{p}'_i^{(0)})\frac{\partial\hat{p}'_i^{(0)}}{\partial\hat{r}}\right] \\ - \frac{\partial}{\partial\hat{z}}\left[\hat{k}_i(\hat{P}_a - \hat{p}'_i^{(0)})\frac{\partial\hat{p}'_i^{(1)}}{\partial\hat{z}}\right] + \frac{\partial}{\partial\hat{z}}\left[\hat{k}_i\hat{p}'_i^{(1)}\frac{\partial\hat{p}'_i^{(0)}}{\partial\hat{z}}\right] = 0. \end{aligned} \quad (4.8)$$

For the boundary conditions along the lens surfaces $\Gamma_i (i = 1, 2)$, pressure continuity from (2.15) gives

$$\hat{p}'_i^{(0)} = \hat{p}'_f^{(0)} \quad \text{on } \Gamma_i (i = 1, 2), \quad (4.9)$$

while flux continuity from (4.6) gives at the first two orders

$$\hat{k}_i\frac{\partial\hat{p}'_i^{(0)}}{\partial\hat{z}} = 0 \quad \text{on } \Gamma_i (i = 1, 2), \quad (4.10)$$

$$-\hat{k}_i\frac{\partial\hat{p}'_i^{(0)}}{\partial\hat{r}}\frac{\partial\hat{F}_i}{\partial\hat{r}} + \hat{k}_i\frac{\partial\hat{p}'_i^{(1)}}{\partial\hat{z}} = \hat{k}_f\left(\frac{\delta_k}{\delta}\right)\frac{\partial\hat{p}'_f^{(0)}}{\partial\hat{z}} \quad \text{on } \Gamma_i (i = 1, 2). \quad (4.11)$$

Also, the zero flux conditions on the bottom and the top boundaries of the coarse zone give

$$\frac{\partial\hat{p}'_i^{(0)}}{\partial\hat{z}} = \frac{\partial\hat{p}'_i^{(1)}}{\partial\hat{z}} = 0 \quad (i = 1, 2, 3) \quad \text{on } \hat{z} = 0 \text{ and } \hat{z} = \hat{d}_3. \quad (4.12)$$

From (4.7) and the boundary conditions (4.10) and (4.12), it is clear that the

leading-order pressure in the coarse zone is uniform in \hat{z} within a layer. Hence,

$$\hat{p}_i^{(0)} = \hat{p}_i^{(0)}(\hat{r}, \hat{t}) \quad (i = 1, 2, 3). \tag{4.13}$$

By this result the last term on the left-hand side of (4.8) vanishes. We next integrate (4.8) with respect to \hat{z} across a particular layer and use Leibniz's rule, the boundary condition (4.12) and the interface conditions (4.9) and (4.11). Specifically, in the bottom coarse layer Ω_1 , the integration is from 0 to $\hat{F}_1(\hat{r})$:

$$\hat{d}_1 \langle \theta_{g1} \rangle \hat{P}_a \frac{\partial \hat{p}_1^{(0)}}{\partial \hat{t}} - \frac{1}{\hat{r}} \frac{\partial}{\partial \hat{r}} \left[\hat{r} \hat{d}_1 \langle \hat{k}_1 \rangle (\hat{P}_a - \hat{p}_1^{(0)}) \frac{\partial \hat{p}_1^{(0)}}{\partial \hat{r}} \right] = \left(\frac{\delta_k}{\delta} \right) \left[\hat{k}_f (\hat{P}_a - \hat{p}_f^{(0)}) \frac{\partial \hat{p}_f^{(0)}}{\partial \hat{z}} \right]_{\hat{z}=\hat{F}_1}. \tag{4.14}$$

In the upper coarse layer Ω_2 , the integration is from $\hat{F}_2(\hat{r})$ to \hat{d}_3 ,

$$\hat{d}_2 \langle \theta_{g2} \rangle \hat{P}_a \frac{\partial \hat{p}_2^{(0)}}{\partial \hat{t}} - \frac{1}{\hat{r}} \frac{\partial}{\partial \hat{r}} \left[\hat{r} \hat{d}_2 \langle \hat{k}_2 \rangle (\hat{P}_a - \hat{p}_2^{(0)}) \frac{\partial \hat{p}_2^{(0)}}{\partial \hat{r}} \right] - \left(\frac{\delta_k}{\delta} \right) \left[\hat{k}_f (\hat{P}_a - \hat{p}_f^{(0)}) \frac{\partial \hat{p}_f^{(0)}}{\partial \hat{z}} \right]_{\hat{z}=\hat{F}_2}. \tag{4.15}$$

In the outer coarse layer Ω_3 , the integration is from 0 to \hat{d}_3 :

$$\langle \theta_{g3} \rangle \hat{P}_a \frac{\partial \hat{p}_3^{(0)}}{\partial \hat{t}} - \frac{1}{\hat{r}} \frac{\partial}{\partial \hat{r}} \left[\hat{r} \langle \hat{k}_3 \rangle (\hat{P}_a - \hat{p}_3^{(0)}) \frac{\partial \hat{p}_3^{(0)}}{\partial \hat{r}} \right] = 0. \tag{4.16}$$

In the above equations, the angle brackets denote depth averages; for example,

$$\langle \hat{k}_1 \rangle(\hat{r}) = \frac{1}{\hat{d}_1} \int_0^{\hat{F}_1} \hat{k}_1(\hat{r}, \hat{z}) d\hat{z}. \tag{4.17}$$

The boundary terms in (4.14) and (4.15) represent leakage into or from the fine-grained lens Ω_f , for which the leading-order flow equation is finally found from (4.5):

$$\theta_{gf} \hat{P}_a \frac{\partial \hat{p}_f^{(0)}}{\partial \hat{t}} - \left(\frac{\delta_k}{\delta} \right) \frac{\partial}{\partial \hat{z}} \left[\hat{k}_f (\hat{P}_a - \hat{p}_f^{(0)}) \frac{\partial \hat{p}_f^{(0)}}{\partial \hat{z}} \right] = 0. \tag{4.18}$$

In summary (4.14)–(4.16) govern the unsteady, essentially horizontal flow in the coarse layers, with leakage from the lens. Equation (4.18) accounts for the essentially vertical flow through the semipervious lens. Thus in all layers the flow equations are just one-dimensional; this simplification is of the same genre as the classical hydrological (quasi-three-dimensional) approximation introduced heuristically by Hantush & Jacob (1955) in the theory of wells in a layered stratum with sharply contrasting permeabilities. Clearly, even without axial symmetry, the present analysis can be modified straightforwardly. The approximate flow would be two-dimensional (horizontal) in the coarse layers, and vertical in the lens. The mathematical saving of the approximation is still considerable.

To solve the above equations, we need the pressure continuity condition (4.9) on the interface, and the following radial boundary conditions as described in §2.2:

$$\frac{\partial \hat{p}_1^{(0)}}{\partial \hat{r}} = 0 \quad \text{at } \hat{r} = 0, \tag{4.19}$$

$$\frac{\partial \hat{p}_2^{(0)}}{\partial \hat{r}} = 0 \quad \text{for } 0 < \hat{t} < \hat{T} \quad \text{and} \quad \hat{p}_2^{(0)} = 1 \quad \text{for } \hat{t} > \hat{T} \quad \text{at } \hat{r} = \hat{r}_0, \tag{4.20}$$

$$\hat{p}_1^{(0)} = \hat{p}_2^{(0)} = \hat{p}_3^{(0)} \quad \text{at } \hat{r} = \hat{r}_b, \quad (4.21)$$

$$\hat{d}_1 \langle \hat{k}_1 \rangle \frac{\partial \hat{p}_1^{(0)}}{\partial \hat{r}} + \hat{d}_2 \langle \hat{k}_2 \rangle \frac{\partial \hat{p}_2^{(0)}}{\partial \hat{r}} = \hat{d}_3 \langle \hat{k}_3 \rangle \frac{\partial \hat{p}_3^{(0)}}{\partial \hat{r}} \quad \text{at } \hat{r} = \hat{r}_b, \quad (4.22)$$

$$\hat{p}_3^{(0)} = 0 \quad \text{at } \hat{r} \rightarrow \infty. \quad (4.23)$$

Once the pressure is solved in various layers, the leading-order specific discharge components can be found from Darcy's law:

$$\langle \hat{u}_i^{(0)} \rangle = \langle \hat{k}_i \rangle \frac{\partial \hat{p}_i^{(0)}}{\partial \hat{r}} \quad (i = 1, 2, 3), \quad (4.24)$$

$$\hat{w}_f^{(0)} = \left(\frac{\delta_k}{\delta} \right) \hat{k}_f \frac{\partial \hat{p}_f^{(0)}}{\partial \hat{z}}. \quad (4.25)$$

If the entire ground surface is unsealed, significant vertical flow will result; the region within a radius of the order of the layer depth \hat{d} from the extraction well will require a fully two-dimensional (\hat{r}, \hat{z}) analysis. If, on the other hand, the ground surface is only sealed (paved) within a radius from the well comparable to the lens radius, the flow in the upper layer below the pavement would still be essentially horizontal and governed by (4.15), while the pressure deviation $\hat{p}_2^{(0)}$ vanishes outside the paved zone. Near the edge of the pavement a locally two-dimensional (\hat{r}, \hat{z}) refinement is needed.

4.2. Chemical vapour transport

4.2.1. Coarse layers

Normalizing the variables according to the scales in table 1, the transport equation (2.5) and the interface condition (2.17) become

$$\begin{aligned} \delta \theta_{gi} \hat{P}_a \frac{\partial \hat{c}_{gi}}{\partial \hat{t}} + \frac{\delta}{\hat{r}} \frac{\partial}{\partial \hat{r}} (\hat{r} \hat{u}_i \hat{c}_{gi}) + \delta \frac{\partial}{\partial \hat{z}} (\hat{w}_i \hat{c}_{gi}) - \frac{\delta}{Pe \hat{r}} \frac{\partial}{\partial \hat{r}} \left(\hat{r} \hat{D}_i \frac{\partial \hat{c}_{gi}}{\partial \hat{r}} \right) - \frac{1}{Pe} \frac{\partial}{\partial \hat{z}} \left(\hat{D}_i \frac{\partial \hat{c}_{gi}}{\partial \hat{z}} \right) \\ = -\delta \frac{6\phi_i \theta_{ai}}{H} \left(\frac{D_{wi} \tilde{r}}{a_i^2 \tilde{u}_c} \right) \sum_{n=1}^{\infty} \int_0^{\hat{t}} e^{-\lambda_{ni}(\hat{t}-\hat{\tau})} \frac{\partial \hat{c}_{gi}}{\partial \hat{\tau}} d\hat{\tau} \quad \text{in } \Omega_i (i = 1, 2, 3), \end{aligned} \quad (4.26)$$

$$\begin{aligned} -\delta \left(\hat{u}_i \hat{c}_{gi} - \frac{\hat{D}_i}{Pe} \frac{\partial \hat{c}_{gi}}{\partial \hat{r}} \right) \frac{\partial \hat{F}_i}{\partial \hat{r}} + \left(\delta \hat{w}_i \hat{c}_{gi} - \frac{\hat{D}_i}{Pe} \frac{\partial \hat{c}_{gi}}{\partial \hat{z}} \right) = -\delta^2 \left(\hat{u}_f \hat{c}_{gf} - \frac{\delta_D \hat{D}_f}{\delta Pe} \frac{\partial \hat{c}_{gf}}{\partial \hat{r}} \right) \frac{\partial \hat{F}_i}{\partial \hat{r}} \\ + \delta \left(\hat{w}_f \hat{c}_{gf} - \frac{\delta_D \hat{D}_f}{\delta Pe} \frac{\partial \hat{c}_{gf}}{\partial \hat{z}} \right) \quad \text{on } \Gamma_i (i = 1, 2), \end{aligned} \quad (4.27)$$

where

$$\hat{\lambda}_{ni} = \lambda_{ni} \tilde{r} / (\tilde{u}_c \hat{P}_a) = n^2 \pi^2 D_{ei} \tilde{r} / (a_i^2 \tilde{u}_c \hat{P}_a) \quad (n = 1, 2, 3, \dots, \quad i = 1, 2, 3). \quad (4.28)$$

Recall from (3.12) and (3.6) that $Pe \geq O(1)$ and $\delta_D = O(\delta)$. Since it has been assumed in (3.16) that the diffusion time in a coarse aggregate is comparable to the advection time, the source term on the right-hand side of (4.26) must be of order δ . Let us now substitute the expansions of \hat{c}_g , \hat{u} and \hat{w} according to (4.1) into (4.26), (4.27) and (2.14). The first two orders of perturbation equations are as follows.

$O(1)$:

$$-\frac{1}{Pe} \frac{\partial}{\partial \hat{z}} \left(\hat{D}_i \frac{\partial \hat{c}_{gi}^{(0)}}{\partial \hat{z}} \right) = 0 \quad \text{in } \Omega_i (i = 1, 2, 3), \tag{4.29}$$

$$-\frac{\hat{D}_i}{Pe} \frac{\partial \hat{c}_{gi}^{(0)}}{\partial \hat{z}} = 0 \quad \text{on } \Gamma_i (i = 1, 2), \tag{4.30}$$

$$\frac{\partial \hat{c}_{gi}^{(0)}}{\partial \hat{z}} = 0 \quad (i = 1, 2, 3) \quad \text{on } \hat{z} = 0 \text{ and } \hat{z} = \hat{d}_3. \tag{4.31}$$

Clearly the above conditions imply that the leading-order concentrations in the coarse layers are independent of \hat{z} . That is,

$$\hat{c}_{gi}^{(0)} = \hat{c}_{gi}^{(0)}(\hat{r}, \hat{t}) \quad (i = 1, 2, 3). \tag{4.32}$$

$O(\delta)$:

$$\begin{aligned} \theta_{gi} \hat{P}_a \frac{\partial \hat{c}_{gi}^{(0)}}{\partial \hat{t}} + \frac{1}{\hat{r}} \frac{\partial}{\partial \hat{r}} (\hat{r} \hat{u}_i^{(0)} \hat{c}_{gi}^{(0)}) + \frac{\partial}{\partial \hat{z}} (\hat{w}_i^{(0)} \hat{c}_{gi}^{(0)}) - \frac{1}{Pe \hat{r}} \frac{\partial}{\partial \hat{r}} \left(\hat{r} \hat{D}_i \frac{\partial \hat{c}_{gi}^{(0)}}{\partial \hat{r}} \right) \\ - \frac{1}{Pe} \frac{\partial}{\partial \hat{z}} \left(\hat{D}_i \frac{\partial \hat{c}_{gi}^{(1)}}{\partial \hat{z}} \right) = A_i \quad \text{in } \Omega_i (i = 1, 2, 3), \end{aligned} \tag{4.33}$$

$$\begin{aligned} - \left(\hat{u}_i^{(0)} \hat{c}_{gi}^{(0)} - \frac{\hat{D}_i}{Pe} \frac{\partial \hat{c}_{gi}^{(0)}}{\partial \hat{r}} \right) \frac{\partial \hat{F}_i}{\partial \hat{r}} + \left(\hat{w}_i^{(0)} \hat{c}_{gi}^{(0)} - \frac{\hat{D}_i}{Pe} \frac{\partial \hat{c}_{gi}^{(1)}}{\partial \hat{z}} \right) \\ = \left(\hat{w}_f^{(0)} \hat{c}_{gf}^{(0)} - \frac{\delta_D \hat{D}_f}{\delta Pe} \frac{\partial \hat{c}_{gf}^{(0)}}{\partial \hat{z}} \right) \quad \text{on } \Gamma_i (i = 1, 2), \end{aligned} \tag{4.34}$$

$$\hat{w}_i^{(0)} = 0, \quad \frac{\partial \hat{c}_{gi}^{(1)}}{\partial \hat{z}} = 0 \quad (i = 1, 2, 3) \quad \text{on } \hat{z} = 0 \text{ and } \hat{z} = \hat{d}_3. \tag{4.35}$$

The phase exchange term on the right-hand side of (4.33) is

$$A_i = -6 \zeta_i \sigma_i \hat{P}_a \sum_{n=1}^{\infty} \int_0^{\hat{t}} e^{-\hat{\lambda}_{ni}(\hat{t}-\hat{\tau})} \frac{\partial \hat{c}_{gi}^{(0)}}{\partial \hat{\tau}} d\hat{\tau} \quad (i = 1, 2, 3), \tag{4.36}$$

where for $i = 1, 2, 3$,

$$\zeta_i = \frac{\phi_i D_{wi} \theta_{ai}}{H D_{ei}} = \frac{[K_{di}(1 - \phi_i) \rho_s + \phi_i] \theta_{ai}}{H}, \tag{4.37}$$

$$\sigma_i = \frac{D_{ei} \tilde{r}}{a_i^2 \tilde{u}_c \hat{P}_a}, \tag{4.38}$$

and

$$\hat{\lambda}_{ni} = n^2 \pi^2 \sigma_i \quad (n = 1, 2, 3, \dots). \tag{4.39}$$

As in the air flow problem, we integrate (4.33) across the three coarse layers, and use Leibniz's rule and the boundary conditions (4.35) or the interface condition (4.34) to get depth-integrated equations. Thus, in the bottom coarse layer Ω_1 , the integration

is from 0 to $\hat{F}_1(\hat{r})$:

$$\begin{aligned} \hat{d}_1 \langle \theta_{g1} \rangle \hat{P}_a \frac{\partial \hat{c}_{g1}^{(0)}}{\partial \hat{t}} + \frac{1}{\hat{r}} \frac{\partial}{\partial \hat{r}} (\hat{r} \hat{d}_1 \langle \hat{u}_1^{(0)} \rangle \hat{c}_{g1}^{(0)}) - \frac{1}{Pe \hat{r}} \frac{\partial}{\partial \hat{r}} \left(\hat{r} \hat{d}_1 \langle \hat{D}_1 \rangle \frac{\partial \hat{c}_{g1}^{(0)}}{\partial \hat{r}} \right) \\ = \hat{d}_1 \langle A_1 \rangle - \left[\hat{w}_f^{(0)} \hat{c}_{gf}^{(0)} - \left(\frac{\delta_D \hat{D}_f}{\delta Pe} \right) \frac{\partial \hat{c}_{gf}^{(0)}}{\partial \hat{z}} \right]_{\hat{z}=\hat{F}_1}. \end{aligned} \quad (4.40)$$

In the upper coarse layer Ω_2 , we integrate from $\hat{F}_2(\hat{r})$ to \hat{d}_3 :

$$\begin{aligned} \hat{d}_2 \langle \theta_{g2} \rangle \hat{P}_a \frac{\partial \hat{c}_{g2}^{(0)}}{\partial \hat{t}} + \frac{1}{\hat{r}} \frac{\partial}{\partial \hat{r}} (\hat{r} \hat{d}_2 \langle \hat{u}_2^{(0)} \rangle \hat{c}_{g2}^{(0)}) - \frac{1}{Pe \hat{r}} \frac{\partial}{\partial \hat{r}} \left(\hat{r} \hat{d}_2 \langle \hat{D}_2 \rangle \frac{\partial \hat{c}_{g2}^{(0)}}{\partial \hat{r}} \right) \\ = \hat{d}_2 \langle A_2 \rangle + \left[\hat{w}_f^{(0)} \hat{c}_{gf}^{(0)} - \left(\frac{\delta_D \hat{D}_f}{\delta Pe} \right) \frac{\partial \hat{c}_{gf}^{(0)}}{\partial \hat{z}} \right]_{\hat{z}=\hat{F}_2}. \end{aligned} \quad (4.41)$$

In the outer coarse layer Ω_3 , the integration is from 0 to \hat{d}_3 :

$$\langle \theta_{g3} \rangle \hat{P}_a \frac{\partial \hat{c}_{g3}^{(0)}}{\partial \hat{t}} + \frac{1}{\hat{r}} \frac{\partial}{\partial \hat{r}} (\hat{r} \langle \hat{u}_3^{(0)} \rangle \hat{c}_{g3}^{(0)}) - \frac{1}{Pe \hat{r}} \frac{\partial}{\partial \hat{r}} \left(\hat{r} \langle \hat{D}_3 \rangle \frac{\partial \hat{c}_{g3}^{(0)}}{\partial \hat{r}} \right) = \langle A_3 \rangle. \quad (4.42)$$

Similar to the flow equations, the transport equations in the three coarse layers (4.40)–(4.42) are radially one-dimensional. The leakage terms in (4.40) and (4.41) couple the transport in Ω_1 and Ω_2 with that in the fine lens Ω_f , which will be discussed in §4.2.2. The radial boundary conditions required to complete the above problem are

$$\frac{\partial \hat{c}_{g1}^{(0)}}{\partial \hat{r}} = 0 \quad \text{at } \hat{r} = 0, \quad (4.43)$$

$$\hat{c}_{g2}^{(0)} = 1 \quad \text{for } 0 < \hat{t} < \hat{T} \quad \text{and} \quad \frac{\partial \hat{c}_{g2}^{(0)}}{\partial \hat{r}} = 0 \quad \text{for } \hat{t} > \hat{T} \quad \text{at } \hat{r} = \hat{r}_0, \quad (4.44)$$

$$\hat{c}_{g1}^{(0)} = \hat{c}_{g2}^{(0)} = \hat{c}_{g3}^{(0)} \quad \text{at } \hat{r} = \hat{r}_b, \quad (4.45)$$

$$\begin{aligned} \hat{d}_1 \left(\langle \hat{u}_1^{(0)} \rangle \hat{c}_{g1}^{(0)} - \frac{\langle \hat{D}_1 \rangle}{Pe} \frac{\partial \hat{c}_{g1}^{(0)}}{\partial \hat{r}} \right) + \hat{d}_2 \left(\langle \hat{u}_2^{(0)} \rangle \hat{c}_{g2}^{(0)} - \frac{\langle \hat{D}_2 \rangle}{Pe} \frac{\partial \hat{c}_{g2}^{(0)}}{\partial \hat{r}} \right) \\ = \hat{d}_3 \left(\langle \hat{u}_3^{(0)} \rangle \hat{c}_{g3}^{(0)} - \frac{\langle \hat{D}_3 \rangle}{Pe} \frac{\partial \hat{c}_{g3}^{(0)}}{\partial \hat{r}} \right) \quad \text{at } \hat{r} = \hat{r}_b, \end{aligned} \quad (4.46)$$

$$\hat{c}_{g3}^{(0)} = 0 \quad \text{at } \hat{r} \rightarrow \infty. \quad (4.47)$$

Also, similar to the flow, if the ground surface is only paved within a radius from the well comparable to the lens radius, the transport in the upper layer underneath the pavement would still be governed by (4.41), while the concentration $\hat{c}_{g2}^{(0)}$ vanishes outside the paved zone. Near the edge of the pavement a locally two-dimensional (\hat{r}, \hat{z}) refinement is needed.

4.2.2. Fine-grained lens

Because of the fine-grained structure of the lens, (2.5) can be greatly simplified. We assume that in the lens the aggregate diffusion time scale is much shorter than the

global advection time scale, or

$$D_{ef}\tilde{t}/a_f^2 = O(\delta^{-1}) \quad \text{so that} \quad \lambda_{nf}\tilde{t} = n^2\pi^2 D_{ef}\tilde{t}/a_f^2 \gg 1 \quad (n = 1, 2, \dots), \quad (4.48)$$

where a_f is the radius of an aggregate and D_{ef} is the sorption-retarded aggregate diffusivity given by (2.7), both for the lens. As shown in Appendix A, the right-hand side of (2.5) can be approximated by the asymptotic expansion (A 2):

$$\text{RHS(2.5)} \sim -\frac{\phi_f D_{wf} \theta_{af}}{H D_{ef}} \left(\frac{\partial c_{gf}}{\partial t} - \frac{a_f^2}{15 D_{ef}} \frac{\partial^2 c_{gf}}{\partial t^2} + \dots \right), \quad (4.49)$$

where D_{wf} is the aqueous diffusivity in an aggregate in the lens. While the leading term above can be combined with the unsteady term on the left-hand side of (2.5), the second term is of the order $a_f^2/(D_{ef}\tilde{t}) (= O(\delta) \ll 1)$ smaller. Using the scales listed in table 1, we may show that to the leading order $O(\delta^0)$,

$$\beta_f \hat{P}_a \frac{\partial \hat{c}_{gf}^{(0)}}{\partial \hat{t}} + \frac{\partial}{\partial \hat{z}} (\hat{w}_f^{(0)} \hat{c}_{gf}^{(0)}) - \frac{\delta_D}{\delta Pe} \frac{\partial}{\partial \hat{z}} \left(\hat{D}_f \frac{\partial \hat{c}_{gf}^{(0)}}{\partial \hat{z}} \right) = 0 \quad (4.50)$$

where β_f is the retardation factor given by

$$\beta_f = \theta_{gf} + \frac{\phi_f D_{wf} \theta_{af}}{H D_{ef}} = \theta_{gf} + \frac{[K_{df}(1 - \phi_f)\rho_s + \phi_f]\theta_{af}}{H} = \theta_{gf} + \xi_f. \quad (4.51)$$

Note that ξ_f is the lens counterpart of ξ_i defined in (4.37). Now, owing to local equilibrium chemical partitioning in aggregates, this term gives rise to retardation of vapour transport in the lens.

Again similar to the flow, the leading-order transport in the fine lens is vertically one-dimensional and the concentration $\hat{c}_{gf}^{(0)}$ depends on \hat{r} only parametrically. The boundary conditions are

$$\hat{c}_{gf}^{(0)} = \hat{c}_{gi}^{(0)} \quad \text{on } \Gamma_i (i = 1, 2). \quad (4.52)$$

So far the approximate equations are valid for soil layers which can be slightly inhomogeneous, in that the soil properties within a layer can depend continuously on space over the scale \tilde{r} horizontally and the scale \tilde{d} vertically.

4.3. Dimensionless parameters

The intensity of well pressure is characterized by the ratio \hat{P}_a given by (3.18). It is larger for a smaller pumping rate, and vice versa. As the pressure deviation in the well ($P_a - p_0$) can be a finite fraction of the atmospheric pressure (P_a), the dimensionless parameter \hat{P}_a is in general of order unity. The Péclet number Pe measures the relative importance of advection over diffusion in the radial transport in the coarse layers where flow is significant. According to its definition in (3.11), Pe is inversely proportional to \hat{P}_a . Several other dimensionless parameters important to the physical and chemical process are discussed below.

(a) Aggregate parameters σ_i , ξ_i ($i = 1, 2, 3$) and β_f

The physical significance of these parameters has been discussed in a previous study (Ng & Mei 1996b). Briefly σ_i , defined in (4.38), is the ratio of advection time to microscopic aggregate diffusion time in a coarse layer, which reflects the depletion rate of a chemical in aggregates relative to the advective transport. It is the key parameter to indicate the departure from local equilibrium of phase partitioning. In the limit of $\sigma_i \gg 1$, local equilibrium exists between aggregate aqueous concentration

and vapour concentration in the air pores. On the other hand, if $\sigma_i \ll 1$, a kinetic situation prevails, i.e. aggregate concentration responds slowly to changes in vapour concentration. The parameter ξ_i , defined in (4.37), is a ratio of chemical mass partitioned in aggregates to that in vapour phase per bulk volume in a coarse layer under equilibrium partitioning. A larger ξ_i corresponds to a greater fraction of the chemical residing in the coarse aggregates, and therefore implies a higher retardation of the transport. The corresponding parameter ξ_f for the lens is a part of the retardation factor $\beta_f = \theta_{gf} + \xi_f$ given by (4.51), as a result of local equilibrium exchange between vapour and aggregate phases in the fine-grained lens. Similarly, a larger β_f means higher partitioning into the aqueous and the sorbed phases, and causes a slower transport in the lens.

(b) Soil-layer properties δ_k/δ and δ_D/δ

The two ratios δ_k/δ and δ_D/δ measure the contrasts in advective and diffusive transport rates respectively, between the fine-grained lens and the coarse layers. If these ratios are small, both advection and diffusion across the lens will take place more slowly than the horizontal transport in the coarse zone. In such a case, the chemical concentration can change relatively fast in the coarse zone, but only modestly in the lens. As a consequence a rapid initial clean-up of the vapour phase in the coarse zone does not guarantee final remediation of the entire soil system, since rebound due to slow diffusion from the lens may continue long after soil venting is stopped.

5. Numerical examples and discussion

We now apply the first-order approximate equations to study the effects of a low-permeability lens on soil vapour extraction. In the following numerical examples, we further assume that the soil within each layer is homogeneous. Therefore the material properties in each layer are constants and equal to their own scales. As a result, all normalized conductivities and diffusivities become 1, i.e. $\hat{k}_i = \hat{k}_f = \hat{D}_i = \hat{D}_f = 1$ where $i = 1, 2, 3$. It is now more convenient to replace the coarse layer subscript $i = 1, 2, 3$ by c , i.e. $\theta_{gi} = \theta_{gc}$, $\sigma_i = \sigma_c$ and $\xi_i = \xi_c$. We also choose the following length scales: $\hat{r} = r_b$ and $\hat{d} = d_3$ so that $\hat{r}_b = \hat{d}_3 = 1$. For the lens geometry, an ellipsoid is chosen whose boundaries are given by

$$\begin{pmatrix} \hat{F}_2(\hat{r}) \\ \hat{F}_1(\hat{r}) \end{pmatrix} = 0.5 \pm 0.1(1 - \hat{r}^2)^{1/2}. \quad (5.1)$$

The lens is centred at the mid-level of the stratum $\hat{z} = 0.5$ and has a maximum thickness of 0.2 at $\hat{r} = 0$. By symmetry about the centreplane of the lens, the thicknesses of Ω_1 and Ω_2 are given by the same function:

$$\hat{d}_1 = \hat{d}_2 = 0.5 - 0.1(1 - \hat{r}^2)^{1/2}. \quad (5.2)$$

The initial boundary value problem is solved numerically by the method outlined in Appendix B. For computational convenience, the inner boundary conditions at $\hat{r} = 0$ are applied at $\hat{r} = \hat{r}_0$ instead. Since a very small \hat{r}_0 is chosen, the error is expected to be insignificant.

Due to the high cost of power the applied well pressure cannot in practice drop below 50% of the atmospheric pressure (Baehr *et al.* 1989). Hence we consider only the range $\hat{P}_a = 20-2$ which is equivalent to $p_0/P_a = 0.95-0.5$. Let us take a typical sand layer for which $\tilde{k}_c P_a / \tilde{D}_c = 100$, which corresponds to a permeability scale

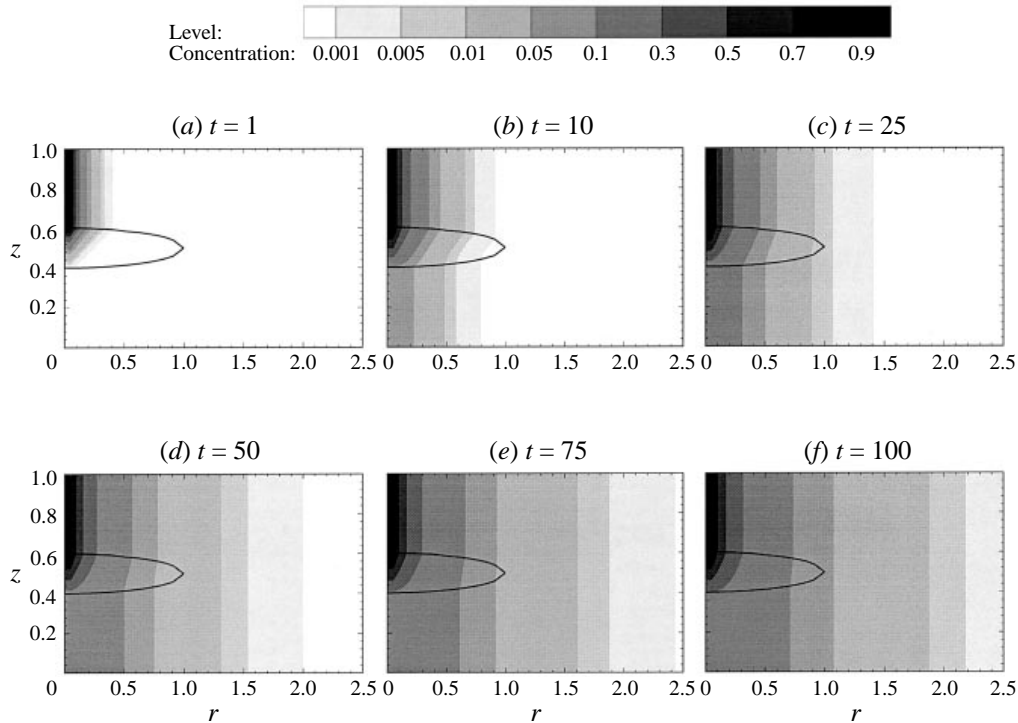


FIGURE 2. Contours of vapour concentration c_g (flood) as a function of time before pumping for Case I: $\delta_k/\delta = 1$, $\delta_D/\delta = 1$, $\sigma_c = 1$, $\beta_f = 5$.

$\tilde{k}_c = O(10^{-8} \text{ m}^2 (\text{Pa s})^{-1})$; the Péclet number is then related to \hat{P}_a by

$$Pe = \tilde{k}_c(P_a - p_0)/\tilde{D}_c = (\tilde{k}_c P_a/\tilde{D}_c)/\hat{P}_a = 100/\hat{P}_a. \quad (5.3)$$

Hence the above range of pumping pressure also corresponds to the range $Pe = 5\text{--}50$.

The initial period of contamination is chosen to be $0 < \hat{t} < \hat{T} = 100$. Pumping begins at $\hat{t} = 100$ and is maintained at a constant rate. To have some idea of the time in reality, if we take a site with a lens radius $\tilde{r} = 30 \text{ m}$, the advection velocity scale is in the range of $\tilde{u}_c = 10^{-6}\text{--}10^{-5} \text{ m s}^{-1}$, according to (3.10). The time scale is $\tilde{t} = O(10)$ days from (3.17). The total time of contamination is roughly three years.

The following input values are chosen for all numerical examples:

$$\hat{r}_0 = 0.05, \quad \theta_{gc} = 0.5, \quad \xi_c = 1, \quad \theta_{gf} = 0.1. \quad (5.4)$$

As sandy materials tend to have a lower sorption coefficient, a relatively small $\xi_c = 1$ is assumed for the coarse layers. On the other hand, clayey materials are usually richer in organic matter and therefore have a larger sorption coefficient. Two values of $\beta_f = 5$ and 50 are considered in the computations. Thus, four sets of values of δ_k/δ , δ_D/δ , σ_c and β_f are chosen for comparison. From now on we shall for simplicity omit the hats and superscripts in all normalized quantities.

5.1. Effects of pumping rate

In Case I we take $\delta_k/\delta = 1$, $\delta_D/\delta = 1$, $\sigma_c = 1$ and $\beta_f = 5$. Figure 2 shows how the chemical vapour spreads in various layers as a function of time before pumping. Clearly the semipervious lens obstructs much of the vapour from diffusing into the

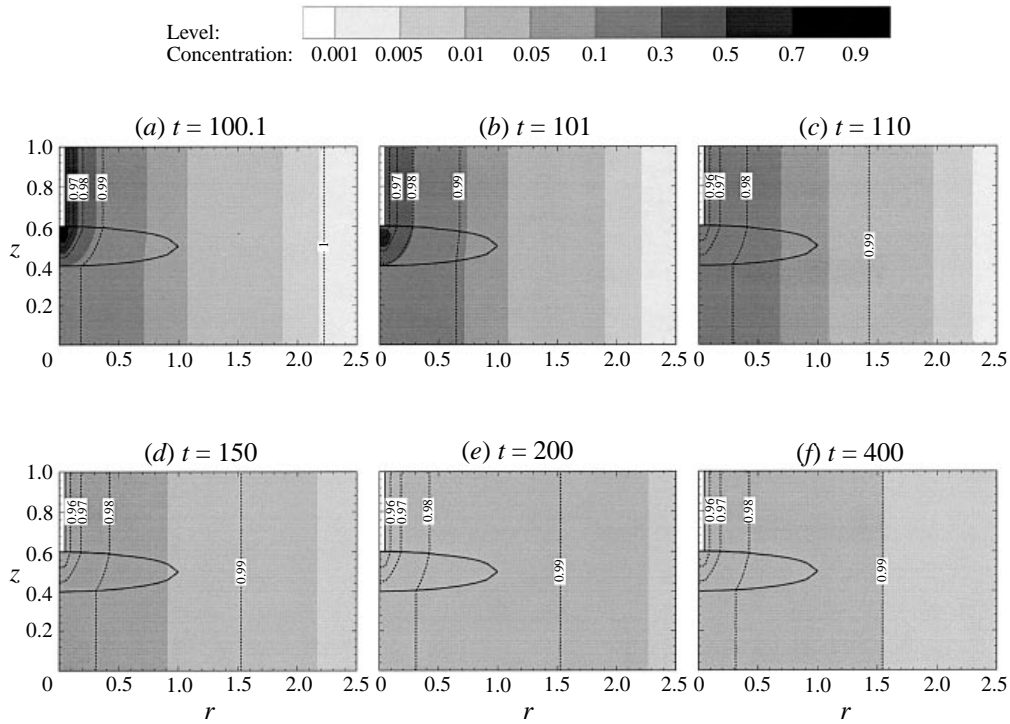


FIGURE 3. Contours of vapour concentration c_g (flood) and air pressure p/P_a (dotted lines) as a function of time during pumping, with $Pe = 5$, for Case I.

bottom layer. Except very far from the centre, there always exists an appreciable concentration gradient across the lens, implying a persistent flux from the top coarse layer to the bottom coarse layer. For example, the maximum vapour concentration in the bottom layer at large times is only 0.3, while that in the top layer is 1.0. While the high concentration levels are confined largely within the upper layer and the lens, the vapour front spreads to a distance more than 2.5 times the lens radius at $t = 100$.

The spatial and temporal variations of the vapour concentration during pumping with two pumping rates $Pe = 5$ and $Pe = 50$ are shown respectively in figures 3 and 4. Also plotted as dotted lines are the contours of the pressure ratio p/P_a , from which the flow development can be inferred. In both cases the flow becomes almost steady when the pumping time is larger than 10 ($t = 110$). Also, beyond this pumping time the concentration gradient across the lens is substantially reduced, resulting in a practically uniform concentration profile across the entire stratum. This is expected since the diffusion time across the lens is of order unity as shown in (3.14). Therefore when pumping is long enough, vertical diffusion is completed, and horizontal advection becomes the major mode of transport in the lens. Clearly, vapour is depleted more rapidly with a higher pumping rate or a stronger advection in all the layers. Note that for the lower pumping rate $Pe = 5$ (figure 3), the vapour concentration at far distances continues to rise with time, despite pumping. This is because far from the well advection is too weak to counter the outward diffusive transport. The situation is reversed only at a very large time when the radial concentration gradient becomes small enough.

Since advection is controlled by the air flow, we show in figure 5 the three specific

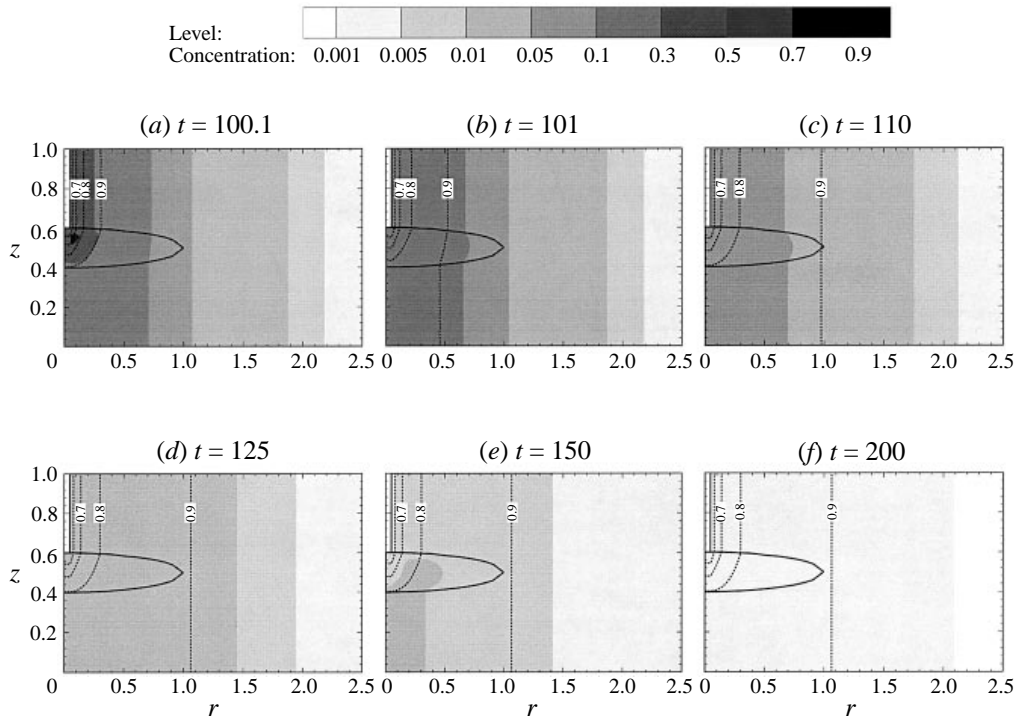


FIGURE 4. Contours of vapour concentration c_g (flood) and air pressure p/P_a (dotted lines) as a function of time during pumping, with $Pe = 50$, for Case I.

discharge components u_1 , u_2 and \bar{w}_f as functions of r at $t = 110$ for the two pumping rates, where \bar{w}_f is the depth-averaged vertical specific discharge in the lens. Note that the horizontal and the vertical components are normalized differently according to table 1. Also note that the scale used in the case $Pe = 50$ is 10 times that in the case $Pe = 5$. Taking this into account, it is clear that when the pressure vacuum in the well increases by 10 times, the velocity components increase at most locations more than 10 times. If the velocity scale \tilde{u}_c has an order of 10^{-5} m s^{-1} as estimated above, the horizontal velocity at the well is then roughly 0.003 mm s^{-1} and 0.05 mm s^{-1} for $Pe = 5$ and $Pe = 50$ respectively. Pumping causes a much higher velocity near the centre in the top layer than in the bottom layer, but the difference diminishes rapidly with radial distance. At a normalized radial distance of 0.5 (i.e. half of the lens radius), both u_2 and \bar{w}_f have already decreased to less than 10% of their maximum values at the well. This explains the long time required to carry vapour farther than this distance, especially in the outer layer, to the pumping well.

It is also of interest to compare (figure 6) the effluent vapour concentration at the well (c_{gw}), with the maximum vapour concentration in the lens (c_{gm}) and the maximum aqueous concentration in the coarse layers (c_{wm}). In the field only the effluent vapour concentration is measured in the well to assess the progress of the clean-up. Clearly a stronger pumping causes the concentration in each layer to reduce very fast at first, and then very slowly in the long run. This tailing effect reflects the slow process of advecting the remote vapour (i.e. that already spread to large radial distances) back to the pumping well. With a stronger pumping the decay curves of the two maximum concentrations are further away from that of the effluent vapour concentration.

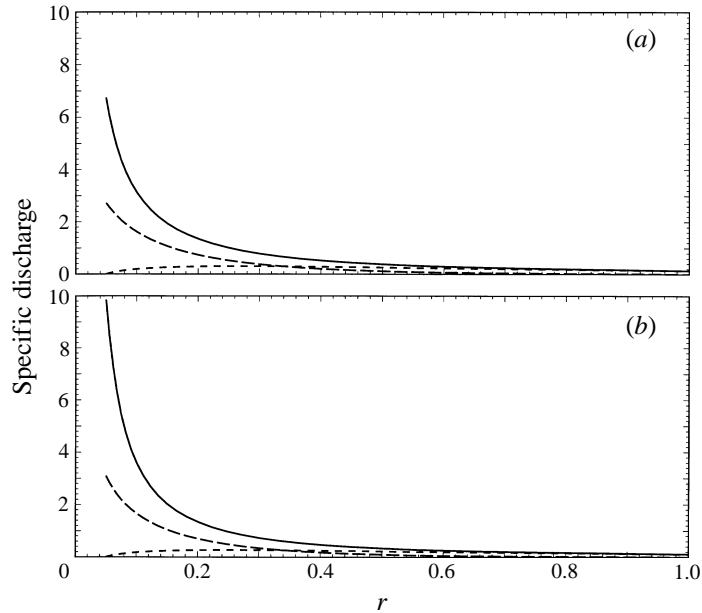


FIGURE 5. Components of specific discharge: u_1 in the bottom layer (short dashes), \bar{w}_f in the lens (long dashes) and u_2 in the upper layer (solid) as a function of radial distance at $t = 110$ for Case I: (a) $Pe = 5$; (b) $Pe = 50$, where the specific discharge scale is 10 times that of (a).

5.2. Effects of lens conductivity and diffusivity

We now consider Case II for a much less pervious lens with $\delta_k/\delta = \delta_D/\delta = 0.1$; the aggregate properties $\sigma_c = 1$, and $\beta_f = 5$ are kept the same. As expected, the lens offers even more resistance to the diffusion of vapour into the bottom layer during the contamination stage (figure 7). The concentration gradient across the lens is more prominent, and the vapour diffuses to the bottom layer through the lens centre and around the lens tip as well (figure 7c). At $t = 100$ the maximum vapour concentration in the lens is only 0.08. The concentration distributions in the outer layer far from the lens are however close to those at the same instant in Case I. This suggests that the effect of the lens diffusivity on the spread of vapour to the outer layer decreases with distance.

We only present the case of large pumping rate ($Pe = 50$) as shown in figure 8. Clearly the concentration in the lens is removed more slowly than for Case I. A lower lens permeability therefore results in a slower response in lens concentration to pumping. For example, when $t = 101$, the maximum concentration in the lens remains as high as 0.8 while that in the top layer has already dropped below 0.2 (figure 8b). However, similar to Case I, the concentration profile across the layers becomes more uniform at larger pumping times.

The effects of a lower lens permeability on the velocity components are shown in figure 9. As compared to figure 5, it can be seen that while the horizontal velocity in the pumping top layer is not much affected, the vertical velocity in the lens and the horizontal velocity in the bottom layer are dramatically reduced. This explains the much weaker advection and therefore slower decay of the vapour concentration in the lens than for Case I.

The time variations of the effluent vapour concentration c_{gw} at the well, the maximum aqueous concentration in coarse layers c_{wm} and the maximum concentration

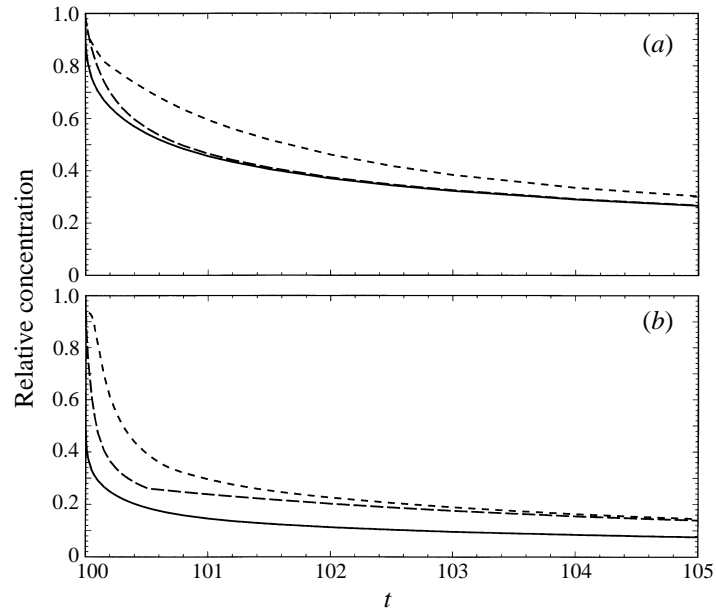


FIGURE 6. Effluent vapour concentration c_{gw} (solid), maximum vapour concentration in the lens c_{gm} (short dashes) and maximum aqueous concentration in the coarse layers c_{wm} (long dashes) as a function of time during pumping for Case I: (a) $Pe = 5$; (b) $Pe = 50$.

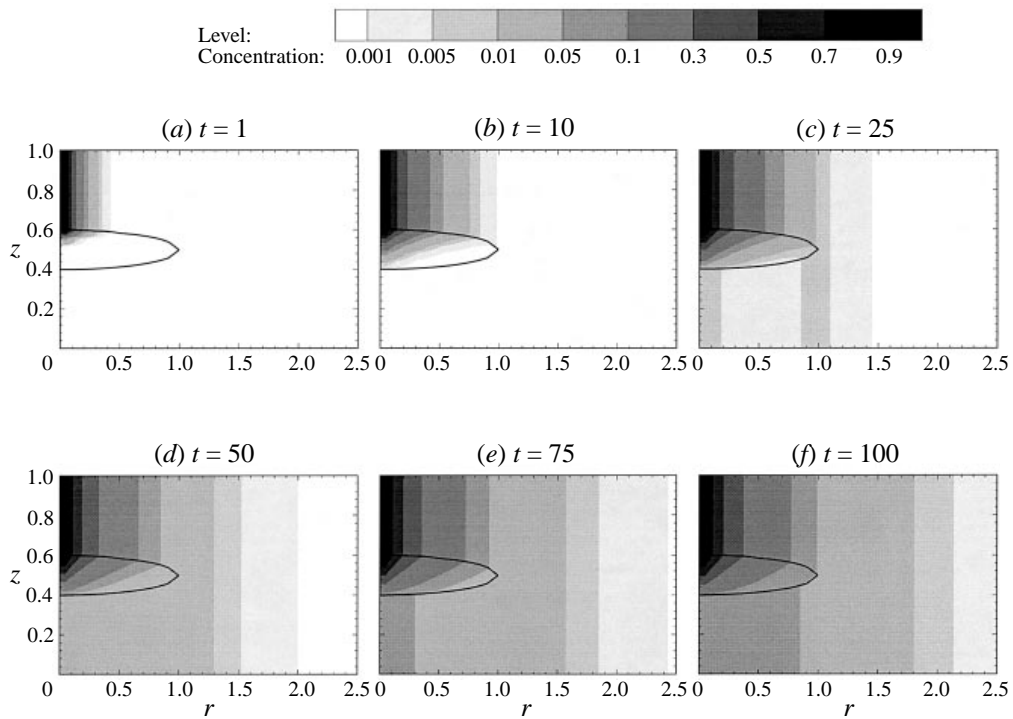


FIGURE 7. Contours of vapour concentration c_g (flood) as a function of time before pumping for Case II: $\delta_k/\delta = 0.1$, $\delta_D/\delta = 0.1$, $\sigma_c = 1$, $\beta_f = 5$.

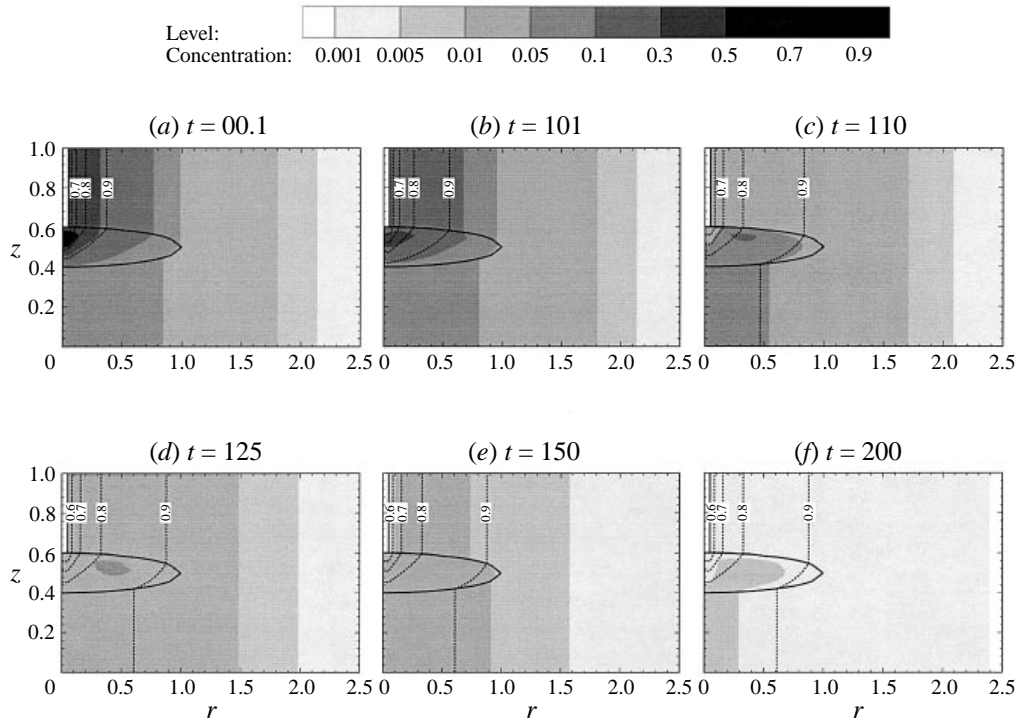


FIGURE 8. Contours of vapour concentration c_g (flood) and air pressure p/P_a (dotted lines) as a function of time during pumping, with $Pe = 50$, for Case II.

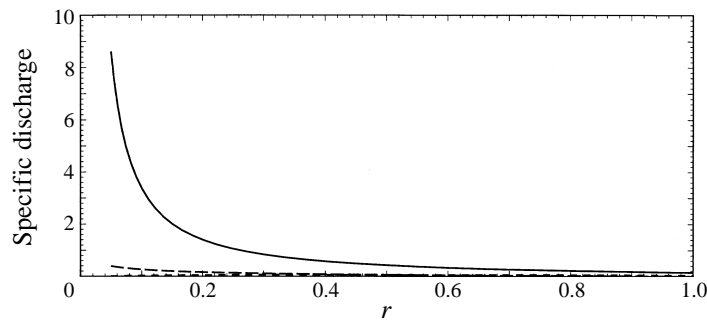


FIGURE 9. Components of specific discharge: u_1 in the bottom layer (short dashes), \bar{w}_f in the lens (long dashes) and u_2 in the upper layer (solid) as a function of radial distance at $t = 110$, with $Pe = 50$, for Case II.

in the lens c_{gm} for Case II are shown in figure 10. While the decay rates for c_{gw} and c_{wm} are close to those in Case I, the slower response of c_{gm} to pumping is obvious. There is a larger difference between the effluent vapour concentration and the maximum concentrations in the soil, especially during the early stage of pumping.

5.3. Effects of aggregate diffusivity

Keeping $\delta_k/\delta = \delta_D/\delta = 0.1$ and $\beta_f = 5$ as in Case II, we examine in Case III the effects of a smaller aggregate diffusion rate $\sigma_c = 0.1$ in the coarse layers. Physically a smaller σ_c implies further departure from local equilibrium between concentrations

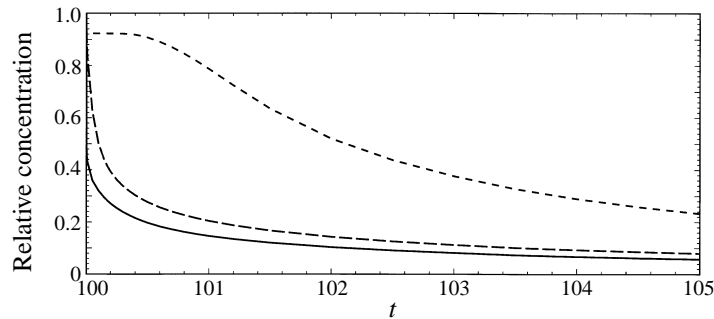


FIGURE 10. Effluent vapour concentration c_{gw} (solid), maximum vapour concentration in the lens c_{gm} (short dashes) and maximum aqueous concentration in the coarse layers c_{wm} (long dashes) as a function of time during pumping, with $Pe = 50$, for Case II.

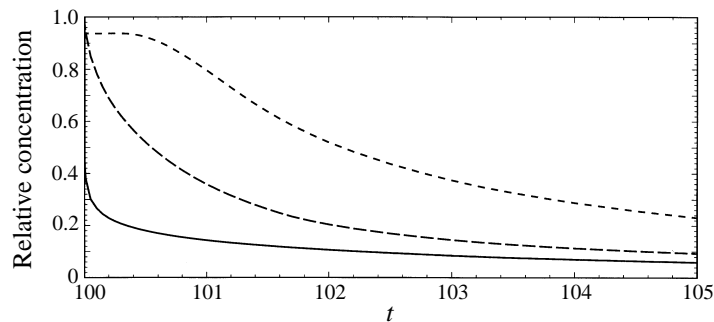


FIGURE 11. Effluent vapour concentration c_{gw} (solid), maximum vapour concentration in the lens c_{gm} (short dashes) and maximum aqueous concentration in the coarse layers c_{wm} (long dashes) as a function of time during pumping, with $Pe = 50$, for Case III: $\delta_k/\delta = 0.1$, $\delta_D/\delta = 0.1$, $\sigma_c = 0.1$, $\beta_f = 5$.

of vapour phase and aqueous phase. However the spread of vapour, during both contamination and pumping stages, is not appreciably different from Case II. This can be illustrated by figure 11 which shows the time changes of c_{gw} , c_{gm} and c_{wm} in Case III. As compared to figure 10, the difference is evident only at the start of pumping when the maximum aqueous concentration now drops more slowly and the effluent vapour concentration drops more abruptly. The difference however diminishes with time when all the concentrations eventually come to the state of tailing. The result is reasonable since the diffusive flux in an aggregate is significant only in a time scale of order unity. Thus the effect of the aggregate diffusion rate is only important in the early stage of pumping. In the long run local phase equilibrium prevails in both coarse and fine soils.

5.4. Effects of lens retardation factor

We now consider in Case IV the effects of the chemical properties in the lens, with the same $\delta_k/\delta = \delta_D/\delta = 0.1$ and $\sigma_c = 0.1$ as Case III, but a larger $\beta_f = 50$, which is increased by a factor of 10. Recall from (4.51) that the retardation factor β_f increases with the sorption partition coefficient which in turn depends on properties of the soil and the chemical. For a higher retardation factor both the advection and the diffusion in the lens are expected to be further slowed down. Figure 12 shows the vapour diffusion before pumping. Now the transport across the lens is so slow that the

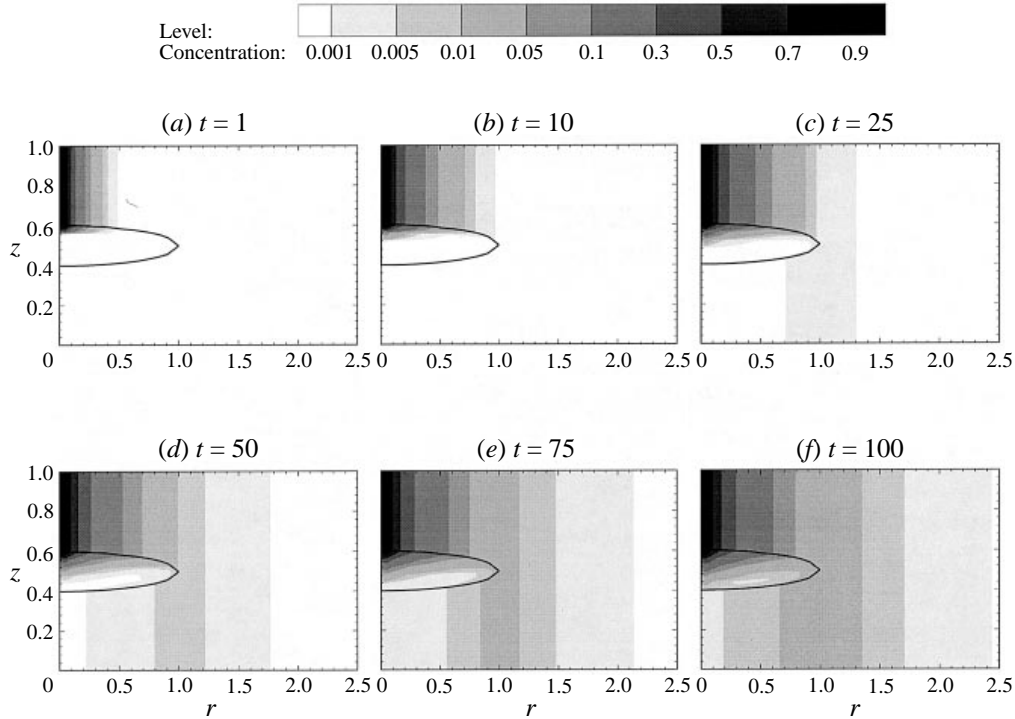


FIGURE 12. Contours of vapour concentration c_g (flood) as a function of time before pumping for Case IV: $\delta_k/\delta = 0.1$, $\delta_D/\delta = 0.1$, $\sigma_c = 0.1$, $\beta_f = 50$.

chemical vapour has to spread outward across the entire radius above the lens before diffusing inward into the bottom layer (figure 12c). The maximum concentration in the bottom layer is now located near the tip of the lens and is less than 0.02 at $t = 100$.

Figure 13 shows how the vapour concentration changes in response to the large pumping rate ($Pe = 50$). Since the travel time is inversely proportional to the retardation factor, the effective transport rate in the lens will be 10 times slower in this case than Case II. The further sluggishness in the attenuation of concentration in the lens is evident as compared to figure 8. During the early period of pumping the maximum vapour concentration in the lens is almost constant in time (figure 14). This case exhibits the largest discrepancy between the decays of the effluent vapour concentration and the maximum concentration in the lens.

5.5. Purge time

To find out how the speed of clean-up depends on the above effects and the pumping pressure, we define the purge time as the time required to reduce the maximum vapour concentration in the lens to 0.01. The results are plotted in figure 15.

For the same Péclet number or pumping intensity, the purge time is obviously longer for a lens of lower permeability (Case II), and longer still for a lens of higher retardation factor (Case IV). A smaller aggregate diffusion rate in the coarse layer (Case III) however has little effect on the purge time. Thus the clean-up rate is basically controlled by the permeability, diffusivity and retardation factor of the lens.

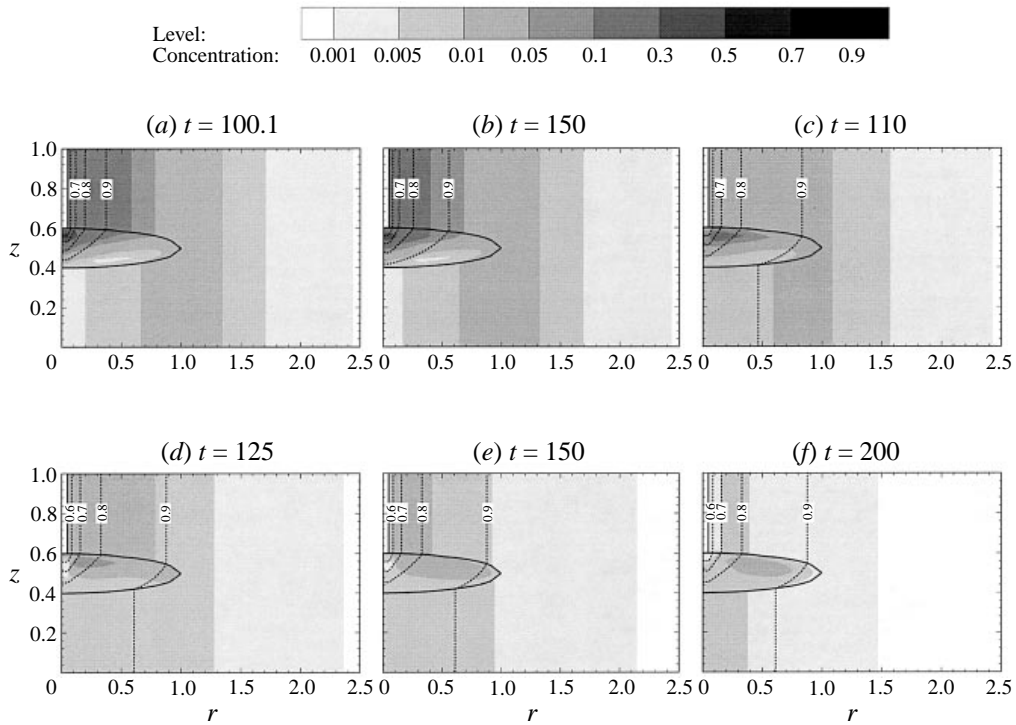


FIGURE 13. Contours of vapour concentration c_g (flood) and air pressure p/P_a (dotted lines) as a function of time during pumping, with $Pe = 50$, for Case IV.

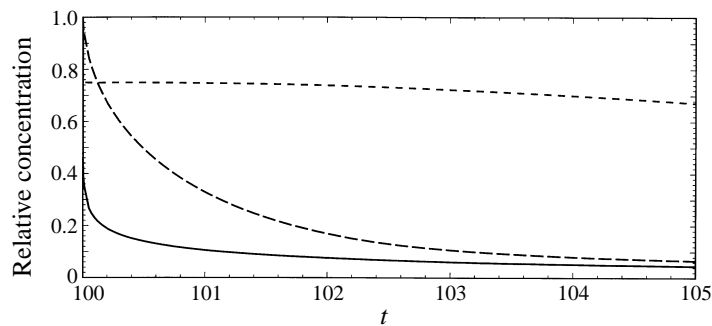


FIGURE 14. Effluent vapour concentration c_{gw} (solid), maximum vapour concentration in the lens c_{gm} (short dashes) and maximum aqueous concentration in the coarse layers c_{wm} (long dashes) as a function of time during pumping, with $Pe = 50$, for Case IV.

Of course the purge time also decreases with increasing vacuum pressure in the well. The reduction is more than 50% as Péclet number increases from 5 to 20. The shortening in purge time however becomes progressively more insignificant when Péclet number increases above 30. Since the cost of pumping depends on both the time and the strength of pumping, it is desirable to clean up the soil in the shortest possible time without an unnecessarily high pumping rate. This is a matter of optimization involving economical factors.

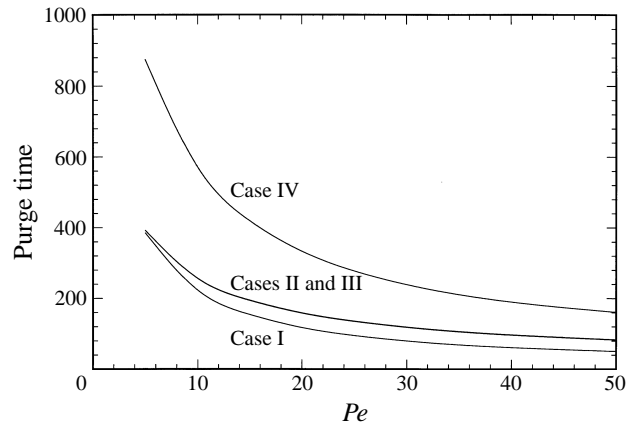


FIGURE 15. Purge time as a function of Pe for Cases I, II, III and IV.

6. Concluding remarks

In this paper we have derived the approximate equations for soil chemical vapour extraction in an unsaturated zone containing a thin lens of low permeability. The key assumptions are (i) the layer thickness is much smaller than the characteristic horizontal length scale; and (ii) there is a sharp contrast between conductivities and diffusivities of the semipervious lens and the coarse layers. The small parameters enable us to perform a perturbation analysis which reduces the dimensions of the governing equations for the air flow and the vapour transport in various layers. Specifically the flow and transport are basically horizontal along the coarse layers and vertical across the lens. While the flow depends on the pressure drop in the well and the permeability ratio, the transport of chemical depends on the Péclet number, the aggregate parameters and the diffusivity ratio. For very permeable soil and strong pumping, advection dominates the transport mechanism.

Results of some numerical computations clarify the significance of the pumping strength and the soil properties. In particular the lens properties (air conductivity and chemical retardation factor) are critical in regulating the rate of vapour removal. Transport across the lens is the slowest in the case of a large retardation factor, low permeability and weak pumping. The aggregate diffusivity in the coarse layer also affects the phase-change kinetics in the early stage of pumping, and becomes less influential in the long run. In all cases the effluent vapour concentration drops more abruptly than the peak concentration in the lens immediately after the start of pumping, but they all exhibit tailing in the long run as the more remote vapour is being extracted.

While a single axisymmetrical lens is treated here, it is straightforward to extend our approximation to more realistic situations where there are several wells and multiple semipervious lenses of general planform. The problem in the coarse layers will be horizontally two-dimensional. Numerical computation will be more demanding but still far less cumbersome than the task of solving a fully three-dimensional problem in all layers. Future development should include the effects of an underlying saturated zone where phase exchange between vapour and the dissolved phase in the groundwater has to be taken into account. Still more challenging is the problem of thermal air-sparging where hot air is injected into the saturated zone to enhance volatilization of the dissolved phase.

It is a pleasure to record our thanks to US Air Force, Office of Scientific Research (Subsurface Contaminant Transport Program, Grant F49620-95-1-0324) for supporting this research.

Appendix A. Asymptotic expansion of the integral source term

In this Appendix we work out the asymptotic expansion of the integral on the right-hand side of (2.5) when the following condition is true:

$$\hat{\lambda}_n = \lambda_n \tilde{t} = n^2 \pi^2 D_e \tilde{t} / a^2 \gg 1 \quad (n = 1, 2, \dots). \tag{A 1}$$

By Laplace’s method, we first approximate the integral by restricting the integration to a narrow region surrounding the maximum of the exponent, $\hat{\tau} = \hat{t}$, about which $\partial c_g / \partial \tau$ can be replaced by its Taylor series. Then the integrals in the series are evaluated after extending the lower integration limit to $-\infty$:

$$\begin{aligned} & \sum_{n=1}^{\infty} \int_0^t e^{-\lambda_n(t-\tau)} \frac{\partial c_g}{\partial \tau} d\tau \\ &= \sum_{n=1}^{\infty} \int_0^{\hat{t}} e^{-\hat{\lambda}_n(\hat{t}-\hat{\tau})} \frac{\partial c_g}{\partial \hat{\tau}} d\hat{\tau} \\ &\sim \sum_{n=1}^{\infty} \int_{\hat{t}-\epsilon}^{\hat{t}} e^{-\hat{\lambda}_n(\hat{t}-\hat{\tau})} \left[\frac{\partial c_g}{\partial \hat{t}} + (\hat{\tau} - \hat{t}) \frac{\partial^2 c_g}{\partial \hat{t}^2} + \dots \right] d\hat{\tau} \quad (\text{for any small } \epsilon > 0) \\ &\sim \sum_{n=1}^{\infty} \int_{-\infty}^{\hat{t}} e^{-\hat{\lambda}_n(\hat{t}-\hat{\tau})} \left[\frac{\partial c_g}{\partial \hat{t}} + (\hat{\tau} - \hat{t}) \frac{\partial^2 c_g}{\partial \hat{t}^2} + \dots \right] d\hat{\tau} \\ &= \sum_{n=1}^{\infty} \frac{1}{\hat{\lambda}_n} \frac{\partial c_g}{\partial \hat{t}} - \sum_{n=1}^{\infty} \frac{1}{\hat{\lambda}_n^2} \frac{\partial^2 c_g}{\partial \hat{t}^2} + \dots \\ &= \frac{a^2}{\pi^2 D_e} \sum_{n=1}^{\infty} \frac{1}{n^2} \frac{\partial c_g}{\partial t} - \frac{a^4}{\pi^4 D_e^2} \sum_{n=1}^{\infty} \frac{1}{n^4} \frac{\partial^2 c_g}{\partial t^2} + \dots \\ &= \frac{a^2}{6D_e} \frac{\partial c_g}{\partial t} - \frac{a^4}{90D_e^2} \frac{\partial^2 c_g}{\partial t^2} + \dots \quad \text{as } \hat{\lambda}_n \gg 1. \end{aligned} \tag{A 2}$$

Appendix B. Numerical method of solution

As noted earlier the flow and the transport problems are mathematically similar, namely the equations are radial in the spatial dimension for the coarse layers, but vertical for the lens. Solutions in the inner coarse layers are coupled to those in the outer coarse layer and in the lens through the continuity conditions on the interfaces. As suggested by these features, we adopt an alternate-direction-iterative finite-difference scheme for both problems. An iterative scheme is required also because the flow equations are nonlinear. Omitting the standard details, we outline the solution scheme as follows.

To give better numerical resolution near the well, we change the radial coordinate by

$$y = \ln(\hat{r} / \hat{r}_0) \tag{B 1}$$

so that

$$\hat{r} \frac{\partial}{\partial \hat{r}} \rightarrow \frac{\partial}{\partial y} \quad \text{and} \quad \frac{1}{\hat{r}} \frac{\partial}{\partial \hat{r}} \left(\hat{r} \frac{\partial}{\partial \hat{r}} \right) \rightarrow \frac{1}{\hat{r}^2} \frac{\partial^2}{\partial y^2}. \quad (\text{B } 2)$$

The coarse layers are linear segments:

$$\left. \begin{array}{l} \Omega_1, \Omega_2 : 0 = y_1 < y < y_b \quad \text{discretized into } I_b - 1 \text{ equal intervals,} \\ \Omega_3 : y_b < y < y_m \quad \text{discretized into } I_m - 1 \text{ equal intervals,} \end{array} \right\} \quad (\text{B } 3)$$

where $y = y_m$ corresponds to a large radial distance at which the far-field boundary conditions are applicable within the time of the problem. On the other hand, the lens is a two-dimensional domain:

$$\Omega_f : \quad 0 = y_1 < y < y_b, \quad \hat{F}_1(y) < \hat{z} < \hat{F}_2(y), \quad (\text{B } 4)$$

which is divided into I_b columns each of which is discretized into J_m equal intervals. The bottom and the top end points of each column in Ω_f coincide respectively with the points in Ω_1 and Ω_2 with the same radial distance. The outer boundary points in Ω_1 and Ω_2 also coincide with the inner boundary point in Ω_3 .

Let the pressure or concentration be known everywhere at $m\Delta t$. Advancing the solutions to $(m+1)\Delta t$ is carried out by the following steps. All individual one-dimensional equations are solved with a standard second-order implicit scheme of forward time, centred-space differences. The integral source terms are calculated with an approximate method described in a previous study (Ng & Mei 1996b).

Step 1. Using the most recent quantities in Ω_f for the interface terms, we first advance solutions by iterations in the three coarse layers satisfying the radial boundary and matching conditions. In each iteration the solutions in Ω_1 and Ω_2 are first obtained with the boundary value at $\hat{r} = \hat{r}_b$ given by that of the last iterate in Ω_3 . The solution in Ω_3 is then found with the flux at \hat{r}_b computed from the new iterates in Ω_1 and Ω_2 . The iterations continue until satisfactory convergence is achieved. For the present study the iteration will stop when the relative difference between two consecutive iterates is less than 10^{-4} for all variables.

Step 2. With the newly obtained solutions in Ω_1 and Ω_2 as the boundary values, we advance solutions in each column (except the one at the lens tip $\hat{r} = \hat{r}_b$) in the lens.

Step 3. Repeat Steps 1 and 2 successively until satisfactory convergence of all solutions is achieved. The convergence criterion is the same as in Step 1.

By now the solution procedure is complete up to $(m+1)$ th time step. The above procedure is repeated for the next time step. The above scheme is applied to both the flow and the transport problems. Nonlinearity in the flow equation is treated by updating the pressure variable in the coefficients at each time of iteration.

REFERENCES

- ABRIOLA, L. M. & PINDER, G. F. 1985 A multiphase approach to the modeling of porous media contamination by organic compounds. 1. Equation development. *Water Resour. Res.* **21**, 11–18.
- ARMSTRONG, J. E., FRIND, E. O. & MCCLELLAN, R. D. 1994 Nonequilibrium mass transfer between the vapor, aqueous, and solid phases in unsaturated soils during vapor extraction. *Water Resour. Res.* **30**, 355–368.
- BAEHR, A. L., HOAG, G. E. & MARLEY, M. C. 1989 Removing volatile contaminants from the unsaturated zone by inducing advective air-phase transport. *J. Contam. Hydrol.* **4**, 1–26.
- BRUSSEAU, M. L. 1991 Transport of organic chemicals by gas advection in structured or heterogeneous porous media: development of a model and application to column experiments. *Water Resour. Res.* **27**, 3189–3199.

- BRUSSEAU, M. L. & RAO, P. S. C. 1990 Modeling solute transport in structured soils: a review. *Geoderma* **46**, 169–192.
- CORAPCIOGLU, M. Y. & BAEHR, A. L. 1987 A compositional multiphase model for groundwater contamination by petroleum products. 1. Theoretical considerations. *Water Resour. Res.* **23**, 191–200.
- FALLOU, S. N., MEI, C. C. & LEE, C. K. 1992 Subsidence due to pumping from layered soil – a perturbation theory. *Intl J. Numer. Anal. Meth. Geomech.* **16**, 157–187.
- FALTA, R. W., JAVANDEL, I., PRUESS, K. & WITHERSPOON, P. A. 1989 Density-driven flow of gas in the unsaturated zone due to the evaporation of volatile organic compounds. *Water Resour. Res.* **25**, 2159–2169.
- FALTA, R. W., PRUESS, K. & CHESNUT, D. A. 1993 Modeling advective contaminant transport during soil vapor extraction. *Ground Water* **31**, 1011–1020.
- GIERKE, J. S., HUTZLER, N. J. & MCKENZIE, D. B. 1992 Vapor transport in unsaturated soil columns: implications for vapor extraction. *Water Resour. Res.* **28**, 323–335.
- HANTUSH, M. S. & JACOB, C. E. 1955 Steady three dimensional flow to a well in a two-layered aquifer. *Trans. Am. Geophys. Union* **36**, 286–292.
- HO, C. K. & UDELL, K. S. 1991 A mass transfer model for the removal of a volatile organic compound from heterogeneous porous media during vacuum extraction. *Heat Transfer in Geophys. Media*. HTD-Vol. 172, pp. 55–62. ASME.
- HO, C. K. & UDELL, K. S. 1992 An experimental investigation of air venting of volatile liquid hydrocarbon mixtures from homogeneous and heterogeneous porous media. *J. Contam. Hydrol.* **11**, 291–316.
- JOHNSON, P. C., KEMBLOWSKI, M. W. & COLTHART, J. D. 1990a Quantitative analysis for the cleanup of hydrocarbon-contaminated soils by in-situ soil venting. *Ground Water* **28**, 413–429.
- JOHNSON, P. C., STANLEY, C. C., KEMBLOWSKI, M. W., BYERS, D. L. & COLTHART, J. D. 1990b A practical approach to the design, operation, and monitoring of in situ soil-venting systems. *Ground Water Monitoring Rev.* **10**, 159–178.
- KALUARACHCHI, J. J. & PARKER, J. C. 1990 Modeling multicomponent organic chemical transport in three-fluid-phase porous media. *J. Contam. Hydrol.* **5**, 349–374.
- LEE, C. K., FALLOU, S. N. & MEI, C. C. 1992 Subsidence due to pumping from a soil stratum with a soft aquitard. *Phil. Trans. R. Soc. Lond. A* **339**, 193–230.
- MENDOZA, C. A. & FRIND, E. O. 1990 Advective-dispersive transport of dense organic vapors in the unsaturated zone, 1. Model development. *Water Resour. Res.* **26**, 379–387.
- MILLINGTON, R. J. 1959 Gas diffusion in porous media. *Science* **130**, 100–102.
- NG, C. O. & MEI, C. C. 1995 Ground subsidence of finite amplitude due to pumping and surface loading. *Water Resour. Res.* **31**, 1953–1968.
- NG, C. O. & MEI, C. C. 1996a Homogenization theory applied to soil vapor extraction in aggregated soils. *Phys. Fluids* **8**, 2298–2306.
- NG, C. O. & MEI, C. C. 1996b Aggregate diffusion model applied to soil vapor extraction in unidirectional and radial flows. *Water Resour. Res.* **32**, 1289–1297.
- RATHFELDER, K., YEH, W. W.-G. & MACKAY, D. 1991 Mathematical simulation of soil vapor extraction systems: model development and numerical examples. *J. Contam. Hydrol.* **8**, 263–297.
- SCHWILLE, F. 1988 *Dense Chlorinated Solvents in Porous and Fractured Media* (translated by J. F. Pankow). Lewis.
- SLEEP, B. E. & SYKES, J. F. 1989 Modeling the transport of volatile organics in variably saturated media. *Water Resour. Res.* **25**, 81–92.
- WILSON, D. J., CLARKE, A. N. & CLARKE, J. H. 1988 Soil clean up by in-situ aeration. I. Mathematical modeling. *Sep. Sci. Technol.* **23**, 991–1037.